

MIT Open Access Articles

Polar liquids at charged interfaces: A dipolar shell theory

The MIT Faculty has made this article openly available. **Please share** how this access benefits you. Your story matters.

Citation: de Souza, J Pedro, Kornyshev, Alexei A and Bazant, Martin Z. 2022. "Polar liquids at charged interfaces: A dipolar shell theory." *The Journal of Chemical Physics*, 156 (24).

As Published: 10.1063/5.0096439

Publisher: AIP Publishing

Persistent URL: <https://hdl.handle.net/1721.1/145497>

Version: Final published version: final published article, as it appeared in a journal, conference proceedings, or other formally published context

Terms of use: Creative Commons Attribution 4.0 International license



Polar liquids at charged interfaces: A dipolar shell theory

Cite as: J. Chem. Phys. **156**, 244705 (2022); <https://doi.org/10.1063/5.0096439>

Submitted: 18 April 2022 • Accepted: 31 May 2022 • Published Online: 29 June 2022

Published open access through an agreement with Massachusetts Institute of Technology

 J.Pedro de Souza,  Alexei A. Kornyshev and  Martin Z. Bazant



View Online



Export Citation



CrossMark

ARTICLES YOU MAY BE INTERESTED IN

Equation of state for confined fluids

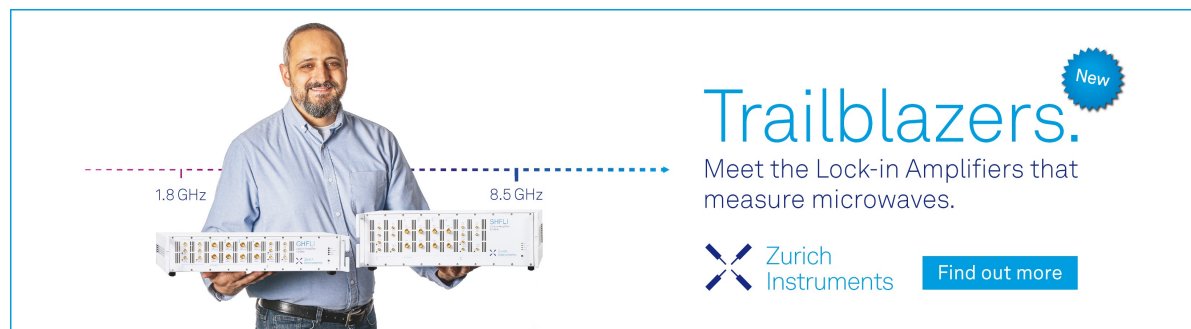
The Journal of Chemical Physics **156**, 244504 (2022); <https://doi.org/10.1063/5.0096875>


On the nature of screening in Voorn–Overbeek type theories

The Journal of Chemical Physics **156**, 244901 (2022); <https://doi.org/10.1063/5.0091721>


“Inner clocks” of glass-forming liquids

The Journal of Chemical Physics **156**, 244506 (2022); <https://doi.org/10.1063/5.0087649>



Trailblazers. 

Meet the Lock-in Amplifiers that measure microwaves.

 Zurich Instruments [Find out more](#)

Polar liquids at charged interfaces: A dipolar shell theory

Cite as: J. Chem. Phys. 156, 244705 (2022); doi: 10.1063/5.0096439

Submitted: 18 April 2022 • Accepted: 31 May 2022 •

Published Online: 29 June 2022



View Online



Export Citation



CrossMark

J. Pedro de Souza,^{1,a)}  Alexei A. Kornyshev,^{2,a)}  and Martin Z. Bazant^{1,3,a)} 

AFFILIATIONS

¹ Department of Chemical Engineering, Massachusetts Institute of Technology, Cambridge, Massachusetts 02142, USA

² Department of Chemistry and Thomas Young Centre for Theory and Simulation of Materials, Imperial College London, Molecular Sciences Research Hub, White City Campus, London W12 0BZ, United Kingdom

³ Department of Mathematics, Massachusetts Institute of Technology, Cambridge, Massachusetts 02142, USA

^{a)} Authors to whom correspondence should be addressed: pdesouza@mit.edu, a.kornyshev@imperial.ac.uk, and bazant@mit.edu

ABSTRACT

The structure of polar liquids and electrolytic solutions, such as water and aqueous electrolytes, at interfaces underlies numerous phenomena in physics, chemistry, biology, and engineering. In this work, we develop a continuum theory that captures the essential features of dielectric screening by polar liquids at charged interfaces, including decaying spatial oscillations in charge and mass, starting from the molecular properties of the solvent. The theory predicts an anisotropic dielectric tensor of interfacial polar liquids previously studied in molecular dynamics simulations. We explore the effect of the interfacial polar liquid properties on the capacitance of the electrode/electrolyte interface and on hydration forces between two plane-parallel polarized surfaces. In the linear response approximation, we obtain simple formulas for the characteristic decay lengths of molecular and ionic profiles at the interface.

© 2022 Author(s). All article content, except where otherwise noted, is licensed under a Creative Commons Attribution (CC BY) license (<http://creativecommons.org/licenses/by/4.0/>). <https://doi.org/10.1063/5.0096439>

I. INTRODUCTION

Polar liquids, such as water, are ubiquitous in all areas of science and engineering, including biological media,^{1,2} electrochemical interfaces,³ colloids,^{4,5} synthetic membranes,^{6,7} and lubrication.^{8,9} At charged interfaces, the structure of polar liquids governs the screening of charge by ions in the electrical double layer.¹⁰ The key and still not fully understood feature here is the interplay between the molecular structure of the solvent and the correlations in ionic subsystems. Theoretical models of interfacial polar liquids are, therefore, critical in the design and understanding of electrified interfaces.

Typically, the dielectric properties of interfacial polar liquids are lumped into two main regions of the electrical double layer: (i) the diffuse layer first described by Gouy and Chapman^{11,12} in which diffuse ionic charges screen the surface charge and (ii) the Stern layer exclusively composed of solvent molecules adjacent to the interface,¹³ represented as a layer of depressed dielectric constant and fixed thickness.¹⁴ In the diffuse layer, the solvent dielectric constant is usually chosen as its bulk value, and the ions are treated

as dilute point charges in the standard Poisson–Boltzmann form. While such a general approach describes numerous electrochemical measurements, the Gouy–Chapman–Stern (GCS) representation does not capture the microscopic details of the structuring of the fluid near the surface^{15–18} nor the electric-field dependent response of the polar solvent.^{19,20} One clear shortcoming of the GCS model is its failure to describe oscillatory profiles seen in hydration force measurements²¹ and x-ray synchrotron-radiation assessed atomic distribution profiles.^{22–24}

A plethora of modifications to the Poisson–Boltzmann theory have been proposed to include the correlated structure and crowding of ions at an interface, usually based on theories of inhomogeneous hard sphere fluids.^{14,25,26} Applications of such theories to electrolytes usually ignore the solvent molecules by treating the fluid as a constant permittivity medium, ϵ , with hard-sphere ions, the so-called primitive model.^{27–29} While such a model can describe the long-range behavior of dilute electrolytes, it does not capture the short-wavelength structuring of the solvent that affects electrostatic interactions between the ions at a nanometer scale.

In fact, simulations and indirect experimental evidence have demonstrated that the bulk dielectric response of water is nonlocal at short distances. Thus, the studied wave-number dependent static dielectric tensor of water has revealed singularities at short wavelengths, giving rise to the phenomenon of overscreening and alternating bound charges of the polar solvent in response to external perturbation.^{30–33} At interfaces, molecular dynamics simulations of interfacial water have shown similar overscreening signatures with singularities in the normal component of the anisotropic static dielectric tensor.^{18,34–38}

To incorporate the dipolar nature of the solvent, a mean-field dipolar Poisson–Boltzmann equation has been developed²⁰ and further extended in Refs. 39–42. These mean-field dipolar models have not yet captured the overscreening signatures of dipolar molecules at interfaces. Theoretical analysis including the overscreening phenomenon by polar liquids has mainly been limited to situations in which the nonlocal permittivity tensor can be included as an input^{43–45} or through effective Landau–Ginzburg models or field theoretic models.^{32,53,46} These approaches, while generally accurate in comparison to simulations and capable of capturing important features of hydration forces, are not derived from the molecular properties of the solvent and require assumptions to match the bulk screening to the interface.

On the other hand, sophisticated molecular theories including the reference interaction site model (RISM) can accurately predict the spatially correlated structures of polar liquids in the bulk and near interfaces.^{47–56} Due to the complexity of the integral equations involved in solving these theories, some of the analytical tractability and physical transparency are lost in favor of model accuracy, compared to local dipolar theories.²⁰ The integral equation theories are, therefore, difficult to incorporate directly with standard continuum dielectric theory approaches.

Clearly, a physically transparent continuum model that incorporates the dipolar, molecular nature of solvent molecules to capture the overscreening behavior at the interface would be useful for understanding the interfacial properties of solvents, solvent mixtures, and electrolytes of varying ionic composition, including at large applied voltages.

Here, we derive a modified Langevin–Poisson equation in which we include the nonlocal dielectric response of a polar liquid by employing a weighted-density functional, treating dipolar molecules as shells of charge. The model captures many of the properties of interfacial liquids, including the overscreening of surface charge by the dipolar solvent charges. Singularities in the normal component of the effective static dielectric permittivity at an interface emerge naturally from the theory. After analyzing pure polar liquids, we, then, include into the theory a finite ion concentration, thus unraveling the fine double layer structure at a charged interface. Furthermore, we apply the theory to describe the hydration forces between two charged surfaces. Finally, we derive a formula for the hydration length, λ_s , which only depends on the diameter of the solvent molecule, d , and the relative permittivity of the liquid, ϵ_r , where $\lambda_s = d\sqrt{(\epsilon_r - 1)/6}$, governing the decay of the oscillations in the bound charge ordering in the polar liquid from a surface. We will explain in this paper the assumptions used to obtain the formula of such extraordinary simplicity, but taken for estimates, it seems to be consistent with existing molecular simulations.^{34,35,38,57,58}

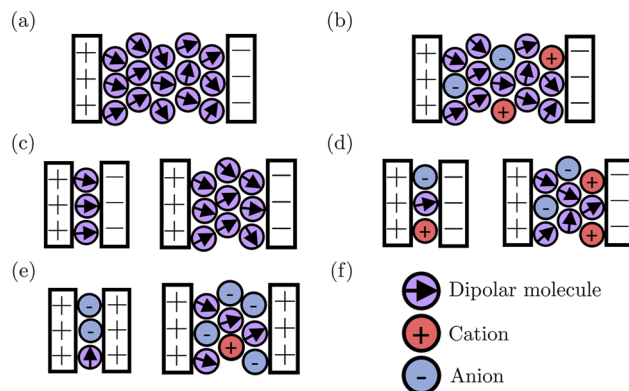


FIG. 1. Schematic of various systems under consideration in the application of the dipolar shell theory. (a) A pure polar fluid between two oppositely charged surfaces of the same magnitude, obeying overall charge neutrality. (b) A 1:1 electrolyte in a polar solvent with ions of the same size as the dipolar molecules, again with surfaces of equal but opposite charge. (c) A confined pure polar fluid with varying extent of confinement between walls of equal but opposite charge with varying extent of confinement. (d) A 1:1 electrolyte confined between two walls of equal but opposite charge with varying extent of confinement. (e) A 1:1 electrolyte confined between two walls of the same charge with varying extent of confinement. (f) Dipolar molecule, cation, and anion symbols.

In this work, we demonstrate the effects of bulk relative permittivity, surface charge density magnitude from linear to nonlinear response, extent of confinement between two surfaces, and ionic concentration on the interfacial properties of the polar liquid. As depicted in Fig. 1, the systems under consideration will include (a) a pure polar liquid between oppositely charged surfaces, (b) an electrolyte between two oppositely charged surfaces, (c) confined pure polar liquids between oppositely charged surfaces, and (d) and (e) confined electrolytes between oppositely charged surfaces and identically charged surfaces, respectively. From our theoretical analysis, we demonstrate the importance of the molecular properties of the polar liquid in hydration interactions and double layer capacitance of charged interfaces.

II. THEORY

The theoretical approach presented here originates from the model developed initially for ionic liquids of Ref. 59, to which we now add dipolar molecules represented by hard spheres with dipolar shells of charge. The model treats the equilibrium properties of a concentrated system of dipolar shells in a manner similar to the Langevin–Poisson theories previously described for point dipoles.²⁰ For simplicity, we limit our analysis to the case of equally sized ions and dipolar molecules. This system of ions and dipoles will be positioned between two flat surfaces. We assume that the dipoles and ions in this nanoslit are in equilibrium with a reservoir with fixed bulk concentrations of both ions and dipoles within the grand canonical ensemble.

A. Density functional

The theoretical framework is based on a definition of the Helmholtz free energy functional of the system and could be classified as a classical density functional theory approach. The Helmholtz

free energy \mathcal{F} can be split into three parts: an ideal part \mathcal{F}^{id} , an excess part accounting for excluded volume effects, \mathcal{F}^{ex} , and an electrostatic part, \mathcal{F}^{el} ,

$$\mathcal{F} = \mathcal{F}^{\text{id}} + \mathcal{F}^{\text{ex}} + \mathcal{F}^{\text{el}}. \quad (1)$$

As a standard definition, the ideal part of the free energy density is given by

$$\mathcal{F}^{\text{id}}[\{c_i(\mathbf{r})\}] = \sum_i k_B T \int d\mathbf{r} c_i(\mathbf{r}) [\ln(\Lambda_i^3 c_i(\mathbf{r})) - 1], \quad (2)$$

where k_B is the Boltzmann constant, T is the absolute temperature, c_i is the concentration of species i , and Λ_i is the de Broglie wavelength for species i . The ideal part of the chemical potential for species i , μ_i^{id} , relative to some reference bulk solution denoted as b , is, thus, given by

$$\beta \mu_i^{\text{id}} = \beta \left(\frac{\delta \mathcal{F}^{\text{id}}}{\delta c_i} - \frac{\delta \mathcal{F}^{\text{id}}}{\delta c_i} \Big|_b \right) = \ln \left(\frac{c_i}{c_{i0}} \right), \quad (3)$$

where c_{i0} is the concentration in the bulk and β is the inverse thermal energy, $\beta^{-1} = k_B T$.

For the excess free energy density, we will assume that all species are approximately spherical and equal in size, of radius R . Here, we adopt a weighted-density approximation from Ref. 59 that was constructed to recover the Carnahan–Starling equation of state,

$$\mathcal{F}^{\text{ex}}[\bar{c}_i(\mathbf{r})] = \frac{k_B T}{v} \int d\mathbf{r} \left[\frac{1}{1 - \bar{\eta}} - 3\bar{\eta} + \frac{1}{(1 - \bar{\eta})^2} \right]. \quad (4)$$

Here, v is the volume of a molecule, $\eta = \sum_i v c_i$ is the local filling fraction, and $\eta_0 = \sum_i v c_{i0}$ is the bulk filling fraction. The bar notation denotes a convolution with the volumetric weighting function, $\bar{\eta} = w_v * \eta$, where $w_v(r) = \Theta(R - |r|)/v$ is a Heaviside step function that only turns on within the volume of the sphere. The $*$ stands for a convolution integral, $f * g = \int d\mathbf{r}' f(\mathbf{r}') g(\mathbf{r} - \mathbf{r}')$. Therefore, the excluded volume interactions appear in a non-local fashion in the chemical potential, describing the filling within a molecular-sized neighborhood of a point. The associated weighted excess chemical potential, $\bar{\mu}_i^{\text{ex}}$, is

$$\begin{aligned} \beta \bar{\mu}_i^{\text{ex}} &= \beta \left(\frac{\delta \mathcal{F}^{\text{ex}}}{\delta c_i} - \frac{\delta \mathcal{F}^{\text{ex}}}{\delta c_i} \Big|_b \right) \\ &= w_v * \left(\frac{8\bar{\eta} - 9\bar{\eta}^2 + 3\bar{\eta}^3}{(1 - \bar{\eta})^3} - \frac{8\eta_0 - 9\eta_0^2 + 3\eta_0^3}{(1 - \eta_0)^3} \right). \end{aligned} \quad (5)$$

B. Derivation of electrostatic variables

The key development in the theory presented in this work is the electrostatic part of the free energy. Here, we spread the ionic charge and bound charges on dipoles over their surface so that they act electrostatically as shells rather than points. The smeared shell charge appears in the mean-field Poisson equation for both the ions and the polar liquid molecules. The charged shell formulation here evolves directly from the theory for concentrated ionic liquids

presented in Ref. 59. The approach was preceded by similar theoretical models for electrolytes composed of ions with intramolecular charge distributions,^{60–65} as well as a charged shell representation of the mean-spherical approximation.^{66–68} The charged shell approximation is applicable not only to ions and dipoles, with charge form factors having the shape of a spherical shell, but also to hard sphere ions and dipoles with point charges and point dipole moments at their centers in which the electrostatic potential can only develop beyond the ionic radius or dipolar molecule radius.

The electrostatic part of the free energy, defined in terms of weighted densities, is, therefore, given by

$$\mathcal{F}^{\text{el}}[\phi, \bar{\rho}_e, \bar{\mathbf{P}}] = \int d\mathbf{r} \left\{ -\frac{\epsilon_0}{2} (\nabla \phi)^2 + \bar{\rho}_e \phi + \bar{\mathbf{P}} \cdot \nabla \phi \right\}, \quad (6)$$

where ϕ is the electrostatic potential, ϵ_0 is the permittivity of free space, $\bar{\rho}_e = w_s * \rho_e$ is the weighted charge density, and $\bar{\mathbf{P}} = w_s * \mathbf{P}$ is the weighted polarization vector, originating from the weighted bound charge on the dipolar molecules, $\bar{\rho}_b = w_s * \rho_b = \nabla \cdot \bar{\mathbf{P}}$. Here, the convolution with the weighting function $w_s(r) = \delta(R - |r|)/(4\pi R^2)$ homogenizes the charge and polarization over a spherical shell.

Using the definition of the polarization vector, \mathbf{P} , as the concentration of dipoles, c_w , multiplied by their individual dipole moments, \mathbf{p} , we can next define the weighted polarization vector, $\bar{\mathbf{P}}$,

$$\mathbf{P} = c_w \mathbf{p}, \quad \bar{\mathbf{P}} = w_s * (c_w \mathbf{p}), \quad (7)$$

for which there will be a distribution of dipole orientations that we will ultimately need to average over. The electrochemical potential of the dipole, μ_w , can be found by taking the variational derivative of the free energy with respect to the dipole concentration,

$$\beta \mu_w = \ln \left(\frac{c_w}{c_{w0}} \right) + \beta \mathbf{p} \cdot \nabla \bar{\phi} + \beta \bar{\mu}_w^{\text{ex}}. \quad (8)$$

Here, $\bar{\phi} = w_s * \phi$ is the weighted electrostatic potential and $\bar{\mu}_w^{\text{ex}} = w_v * \mu_w^{\text{ex}}$ is the weighted excess chemical potential. Mathematically, the weighted electrostatic potential and weighted excess chemical potential emerge due to the minimization of the free energy with respect to the concentration variables, which are present in the free energy in terms of convolutions with weighting functions. Physically, these are a result of the delocalization of bound charge over the dipolar molecule surface and the nonlocal packing effects, respectively. This procedure embeds the finite size of dipolar molecules into the theory, which plays a key role in capturing the effects of layering and decoupling the packing periodicity from the longer range electrostatic correlations. Thus, although this approach should still be classified as a mean field theory, it makes an essential step toward accounting for the molecular structure of the liquid. The dipole concentration at a given position is, thus, given by

$$c_w = c_{w0} \exp(-\beta \mathbf{p} \cdot \nabla \bar{\phi} - \beta \bar{\mu}_w^{\text{ex}}). \quad (9)$$

Therefore, the local dipole concentration depends on the angle, θ , between the dipole moment of the molecule and the weighted electric field, $\bar{\mathbf{E}} = w_s * \mathbf{E} = -\nabla \bar{\phi}$, where

$$\mathbf{p} \cdot \nabla \bar{\phi} = p_0 |\nabla \bar{\phi}| \cos \theta, \quad (10)$$

assuming a constant effective dipole moment magnitude, p_0 . Averaging over the possible orientations of the molecule gives

$$\langle c_w \rangle = c_{w0} e^{-\beta \bar{\mu}_w^{\text{ex}}} \left\langle e^{-\beta p_0 |\nabla \bar{\phi}| \cos \theta} \right\rangle \quad (11)$$

for the dipole concentration and

$$\langle \mathbf{P} \rangle = c_{w0} p_0 e^{-\beta \bar{\mu}_w^{\text{ex}}} \frac{\nabla \bar{\phi}}{|\nabla \bar{\phi}|} \left\langle \cos(\theta) e^{-\beta p_0 |\nabla \bar{\phi}| \cos \theta} \right\rangle \quad (12)$$

for the polarization vector, where $\langle \rangle$ denotes the average over θ . Averaging over the dipole orientations gives

$$\begin{aligned} \left\langle e^{-\beta p_0 |\nabla \bar{\phi}| \cos \theta} \right\rangle &= \frac{1}{2} \int_0^\pi e^{-\beta p_0 |\nabla \bar{\phi}| \cos \theta} \sin \theta d\theta \\ &= \frac{\sinh(\beta p_0 |\nabla \bar{\phi}|)}{\beta p_0 |\nabla \bar{\phi}|} \end{aligned} \quad (13)$$

and

$$\begin{aligned} \left\langle \cos(\theta) e^{-\beta p_0 |\nabla \bar{\phi}| \cos \theta} \right\rangle &= \frac{1}{2} \int_0^\pi e^{-\beta p_0 |\nabla \bar{\phi}| \cos \theta} \cos \theta \sin \theta d\theta \\ &= -\frac{\sinh(\beta p_0 |\nabla \bar{\phi}|)}{\beta p_0 |\nabla \bar{\phi}|} \mathcal{L}(\beta p_0 |\nabla \bar{\phi}|), \end{aligned} \quad (14)$$

where $\mathcal{L}(x) = \coth(x) - 1/x$ is the Langevin function. Therefore, the dipole concentration can be written as

$$\langle c_w \rangle = c_{w0} e^{-\beta \bar{\mu}_w^{\text{ex}}} \frac{\sinh(\beta p_0 |\nabla \bar{\phi}|)}{\beta p_0 |\nabla \bar{\phi}|}, \quad (15)$$

and the polarization density can be expressed as

$$\langle \mathbf{P} \rangle = -p_0 \langle c_w \rangle \frac{\nabla \bar{\phi}}{|\nabla \bar{\phi}|} \mathcal{L}(\beta p_0 |\nabla \bar{\phi}|). \quad (16)$$

In turn, the weighted polarization vector is defined as

$$\langle \bar{\mathbf{P}} \rangle = -w_s * \left[p_0 \langle c_w \rangle \frac{\nabla \bar{\phi}}{|\nabla \bar{\phi}|} \mathcal{L}(\beta p_0 |\nabla \bar{\phi}|) \right]. \quad (17)$$

Moving forward, we drop the bracket notation such that \mathbf{P} refers to $\langle \mathbf{P} \rangle$, $\bar{\mathbf{P}}$ refers to $\langle \bar{\mathbf{P}} \rangle$, and c_w refers to $\langle c_w \rangle$.

Along with the description of the polarization vector, we must also describe the ionic charge when there is a non-zero electrolyte concentration. The ionic electrochemical potential is defined as

$$\beta \mu_i = \ln \left(\frac{c_i}{c_{i0}} \right) + z_i e \beta \bar{\phi} + \beta \bar{\mu}_i^{\text{ex}}. \quad (18)$$

Therefore, the distributions of the ions are given by

$$c_i = c_{i0} \exp(-\beta e \bar{\phi} - \beta \bar{\mu}_i^{\text{ex}}). \quad (19)$$

For a 1:1 solution of concentration c_0 , the electrolyte charge density is, therefore, given as follows:

$$\rho_e = -2ec_0 \sinh(\beta e \bar{\phi}) e^{-\beta \bar{\mu}_i^{\text{ex}}}, \quad (20)$$

and the weighted electrolyte charge density is $\bar{\rho}_e = w_s * \rho_e$.

The Poisson equation consistent with the free energy density in Eq. (6) is

$$-\epsilon_0 \nabla^2 \bar{\phi} = -\nabla \cdot \bar{\mathbf{P}} + \bar{\rho}_e, \quad (21)$$

as shown in Appendix A. The overall charge density in the Poisson equation includes both the weighted bound charge density on the dipolar molecules, $\bar{\rho}_b = -\nabla \cdot \bar{\mathbf{P}}$, and the weighted ionic charge, $\bar{\rho}_e$.

C. Reducing to one dimension

In the 1D geometry between two flat plates, the weighting function formulas can be modified⁶⁹ to integrate over the y and z dimensions since all variables depend only on x . Physically, the spherical shell of charge corresponding to w_s becomes equivalent to a line of charge with length $2R$ and uniform charge per length (the differential area of a sphere per differential in the axial coordinate). The spherical Heaviside weighting function, w_v , becomes a quadratic function, corresponding to the differential volume of a sphere per differential in the axial coordinate. Their modified forms are as follows:

$$w_v(x-x') = \frac{\pi(R^2 - (x-x')^2)}{v} \Theta(R - |x-x'|), \quad (22)$$

$$w_s(x-x') = \frac{1}{2R} \Theta(R - |x-x'|). \quad (23)$$

In 1D, the integro-differential equation for the electrostatic potential is

$$0 = \epsilon_0 \frac{d^2 \bar{\phi}}{dx^2} - \frac{d\bar{P}}{dx} + \bar{\rho}_e, \quad (24)$$

where

$$P = -p_0 c_{w0} e^{-\beta \bar{\mu}_w^{\text{ex}}} \frac{\sinh(\beta p_0 \bar{\phi}')}{\beta p_0 \bar{\phi}'} \mathcal{L}(\beta p_0 \bar{\phi}'), \quad (25)$$

and $\bar{\phi}' = d\bar{\phi}/dx$ denotes a derivative with respect to x . In this geometry, the average orientation of the dipoles relative to the x axis can be expressed as

$$\langle \cos(\theta) \rangle = -\mathcal{L}(\beta p_0 \bar{\phi}'). \quad (26)$$

We assume that the surface charge is uniformly distributed on bounding flat hard walls at $x = 0$ and $x = L$. For simplicity, here, the

surface charge density is assumed not to have any finite size, so the boundary conditions reduce to

$$\begin{aligned} (-\epsilon_0\phi')|_{x=0} &= q_s, \\ (-\epsilon_0\phi')|_{x=L} &= \pm q_s, \end{aligned} \quad (27)$$

where we have the surface charge density of magnitude q_s on each side. Depending on the scenario under investigation, the charge on each surface is either opposite in sign or the same in sign, as sketched in Fig. 1. If the charge at $x = L$ is negative, we choose “+” in the second line of Eq. (27), and the opposite is true if the charge is positive. The local dipolar and ionic concentrations are zero in the regions $x < R$ and $x > L - R$ owing to the hard sphere repulsion from the flat bounding surfaces. To solve these equations, we discretized them using finite difference formulas.

D. Extracting the effective local dielectric tensor

A fundamental calculation involves extracting the static dielectric tensor profile from the predicted polarization vector. Here, we choose a permittivity definition that is consistent with the weighted Poisson equation. First, we directly define the normal component based on the solution to the 1D equations we posed. We then seek a perturbative estimate of the tangential component from the 1D solution.

1. Normal component

The self-consistent definition of the normal permittivity is given by

$$\epsilon_{\perp} = 1 - \frac{\bar{P}}{\epsilon_0\phi'}, \quad (28)$$

which represents the total displacement vector, $D = -\epsilon_0\phi' + \bar{P}$, divided by the electric field, both extracted directly from our model. Note that while the electrochemical potential of the dipoles depends on the weighted electrostatic field, the displacement vector includes a contribution from the local electric field ($-\phi'$) and also the weighted polarization vector (\bar{P}). The modified Poisson equation can be written in terms of the effective normal permittivity in the following form:

$$\frac{d}{dx} \left(\epsilon_0\epsilon_{\perp} \frac{d\phi}{dx} \right) = -\bar{\rho}_e. \quad (29)$$

Here, the effective normal permittivity includes only the polarization of the solvent and does not include the polarization from the ions. We will return to the nuances of the definition of the normal permittivity in the analysis of concentrated electrolytes.

2. Tangential component

While we assume no tangential component of the field in the solution of our model, we can also use the model to quantify the extent of tangential polarizability of the interfacial polar liquid in response to macroscopic electric fields tangential to the plane of the interface. If the tangential electric field is constant and weak relative to the normal electric field, then we can extract it as a small, constant perturbation upon the normal field. For example, we can assume a small perturbative component of the electric field in the y direction, E_y , which satisfies $|E_y| \ll |E_x|$. We can approximate the

magnitude of the gradient of the weighted electrostatic potential as $|\nabla\phi| \approx |\bar{E}_x| = |\bar{\phi}'|$, where the prime notation still refers to derivatives in the x -direction and \bar{E}_x is the weighted electric field in the x -direction. If we apply such an assumption to the y -component of Eq. (17), the displacement vector in the y -direction is, therefore, as follows:

$$\begin{aligned} D_y &= \epsilon_0 E_y + \bar{P}_y \approx \epsilon_0 E_y + w_s * \left[p_0 c_w \frac{\bar{E}_y}{|\bar{E}_x|} \mathcal{L}(\beta p_0 |\bar{E}_x|) \right] \\ &\approx \epsilon_0 E_y + w_s * \left[p_0 c_w \frac{\bar{E}_y}{\bar{\phi}'} \mathcal{L}(\beta p_0 \bar{\phi}') \right]. \end{aligned} \quad (30)$$

Next, we divide the tangential (y) component of the displacement vector by the tangential electric field (E_y). Since we assume that the tangential electric field is constant due to the system's translational invariance in the yz -plane, it can be treated as a constant for the differentiation or convolution operations so that $E_y \approx \bar{E}_y$. Through this process, the tangential permittivity, ϵ_{\parallel} , can be defined as

$$\epsilon_{\parallel} \approx 1 - w_s * \left(\frac{P}{\epsilon_0\bar{\phi}'} \right). \quad (31)$$

III. RESULTS

The equations are solved between two surfaces with fixed charge densities of magnitude q_s and separation distance L . The baseline parameters correspond to the effective values for water: dipolar molecule concentration $c_{w0} = 55\text{M}$ (corresponding to ≈ 33 molecules per nm^3), temperature $T = 300\text{K}$, and a diameter of $d = 0.285\text{nm}$. While ϵ_r is the bulk dielectric constant far from the interface, the local static dielectric tensor can vary as a function of position. In the bulk, the relative permittivity as given by the dipolar model for small perturbations is given by²⁰

$$\epsilon_r = 1 + \frac{\beta c_{w0} p_0^2}{3\epsilon_0}. \quad (32)$$

For a dipolar concentration of $c_{w0} = 55\text{M}$ at $T = 300\text{K}$, the bulk dielectric constant of $\epsilon_r = 80$ requires an effective dipole moment of $p_0 = 4.86\text{D}$. This effective value is significantly larger than the actual molecular dipole moment in the liquid water phase, $2.95 \pm 0.2\text{D}$.⁷⁰ The effective dipole moment, p_0 , accounts for correlations between the orientation of a single dipolar molecule and the orientation of its nearest neighbors, as accounted for in more sophisticated bulk dielectric theories.^{39,71–73} In those theories, a Kirkwood G-factor rescales the effective dipole moment to capture the dipole–dipole correlations, as studied extensively in previous studies of bulk⁷⁴ and confined water.⁵⁷ Once an effective dipole moment is chosen in our theory, the relevant quantities that determine the charge ordering at the interface are mean-field or no local convolutions of mean-field variables so that the dipole–dipole correlations are not double counted. Therefore, we lump these effects into the effective dipole moment in our model, similar to previous dipolar Poisson–Boltzmann approaches.^{20,42} The default separation distance between the two charged surfaces is $L = 5\text{nm}$, and the default surface charge density magnitude is $q_s = 0.01\text{C/m}^2$.

With the inclusion of the polar fluid, the parameter space for the system under investigation is large. We, therefore, divide our results into five parts: (A) First, we present results for pure polar fluids between two opposite surfaces. We formally investigate how the interfacial electrostatic properties change with varying bulk dielectric constant and also how nonlinear saturation of the dipole orientation arises at high surface charge. We also show the complicated layering of the molecular orientation for dipolar fluids confined to the sub-nanometer scale. (B) Second, the interfacial electrostatic properties are investigated with a non-zero ionic concentration between oppositely charged surfaces. Here, the results are presented for varying ionic concentrations and for varying surface charge magnitudes. (C) Next, the theory is applied to understanding hydration interactions between two surfaces of (i) opposite charge with and without ions present and (ii) the same charge with a non-zero ionic concentration. (D) The double layer capacitance with ions present is, then, investigated, ensuring non-overlapping double layers with large separation distances between the surfaces. (E) Finally, the equations are linearized and cast into a differential form, which gives analytical expressions for decay lengths describing the layering of charge and mass at the interface.

A. Pure polar fluids: Interfacial dielectric structure

The system of a pure polar fluid is rare, in practice, but it is a useful reference system to show the dipolar shell theory predictions. In order to maintain electroneutrality, the bounding surfaces must have equal but opposite charge density since the pure polar fluid does not have any net charge. Within this system, we will highlight the influence of the fluid bulk permittivity, ϵ_r , the strength of the electric field in the system that is set by the surface charge density on the boundaries, q_s , and the confinement extent of the fluid given by the surface separation distance, L .

To start, we investigate the effect of the effective dipole moment, p_0 , on the resulting potential and electric field distribution. Since p_0 , of course, determines the bulk macroscopic dielectric constant, ϵ_r , we may say that we will trace the effect of the latter on the local properties near the interface, although the variation ϵ_r is itself the result of variation of p_0 . In order to study fluids of different bulk dielectric constants, we vary p_0 to take on the values $p_0 = 2.36$ D for $\epsilon_r = 20$ and $p_0 = 1.09$ D for $\epsilon_r = 5$, keeping all other variable constant.

In Fig. 2, the electrostatic potential, electric field, and polarization density are plotted along with their weighted counterparts for fluids of varying bulk permittivity, ϵ_r . For each fluid, the electrostatic potential, ϕ , oscillates near the surface, within the first nanometer. The potential difference across the nanoslit is greatest for the least polar fluid with $\epsilon_r = 5$ since the dielectric screening is the weakest for this system. The oscillations in the potential lead to sharp cusps and oscillations in the electric field, E , for all three studied fluids. The electric field even reverses signs at some points, corresponding to *overscreening* of the surface charge. The oscillations and sign reversals in the electric field are stronger for the more polar fluids with higher ϵ_r . The local polarization density, P , has related signatures, where the local polarization density magnitude exceeds the imposed displacement field magnitude set by the surface charge density on the bounding walls. For the weighted variables, $\bar{\phi}$, \bar{E} , and \bar{P} , the weighting operation smoothens out the oscillations compared to the local variables, but does not eliminate them.

The weighted electrostatic potential, $\bar{\phi}$, and weighted electric field, \bar{E} , determine the local electrostatic energy and orientation of the dipolar shells in the theory. The weighted polarization density, \bar{P} , contributes to the overall displacement field, $D = \epsilon_0 E + \bar{P}$. Therefore, the overscreening of the surface charge occurs when \bar{P} exceeds q_s , where the cumulative bound dipolar shell charge exceeds the surface charge density. All three studied the fluids experience at least one overscreening peak in the weighted polarization profile. However, the oscillations decay more rapidly and the overscreening peaks are smaller for the lower bulk permittivity liquids. From these profiles, we can deduce that the overscreening is essential to describing the structuring of polar liquids with large bulk dielectric constant and is sensitive to the effective dipole moment, p_0 .

Next, we can use the electrostatic variables to determine the components of the dielectric tensor near the interface, as shown in Fig. 3, for fluids with different bulk dielectric constants. Due to the weighted polarization density overscreening of the surface charge density, the normal component of the dielectric tensor has singularities. The tangential component, on the other hand, does not have the same overscreening structure since it is set by a long range tangential electric field, and the tangential component of the dielectric function varies closely with the local dipole concentration, c_w . The orientation of the dipoles, $\langle \cos(\theta) \rangle$, is actually higher for the fluid that is the least polar. This fact appears because the least polar fluid with $\epsilon_r = 5$ corresponds to the weakest dielectric screening of the electric field. Even though large differences are observed in the dielectric profiles, at the low charge density of $q_s = 0.01$ C/m², the dipole concentration is not very strongly affected by electrostatics, as shown in Fig. 3(d). Instead, the dipole density is dominated by the packing effects embedded in $\bar{\mu}_i^{\text{ex}}$, which is independent of electrostatics at small potentials.

The large contact value for the density is also governed by the nonlocal packing effects, similar to uncharged hard-sphere fluids. In turn, the excess chemical potential owing to packing plays a minor role in the overscreening structure in the normal component of the dielectric tensor. The overscreening signatures can, therefore, be attributed to the delocalization of the bound charge on dipoles over the dipole molecule surface. The remarkable anisotropic static dielectric tensor predicted by the dipolar shell theory here is similar to the reported molecular dynamics simulations of the dielectric properties of interfacial water.^{18,35,38,57,58} The overscreening signatures also qualitatively match the results from simulations and a phenomenological electrostatic theory of confined liquids.⁷⁵

Furthermore, we explore what happens when a pure polar fluid with bulk dielectric constant $\epsilon_r = 80$ is subjected to a strong electric field at the boundaries, driving the system to nonlinear response with experimentally feasible surface charge densities. Figure 4 includes the normal dielectric permittivity, the tangential permittivity, the dipole orientation, and the dipole density as a function of distance from the left surface for different values of surface charge density. The overscreening structure and singularities in the normal dielectric constant are more or less unchanged as the surface charge increases. However, at the largest charge density, $q_s = 0.25$ C/m², the normal and tangential components of the permittivity saturate to a lower value. Even though the strong electric field leads to dielectric saturation and electrostriction (an increase in the local dipolar concentration near the interface), the saturation

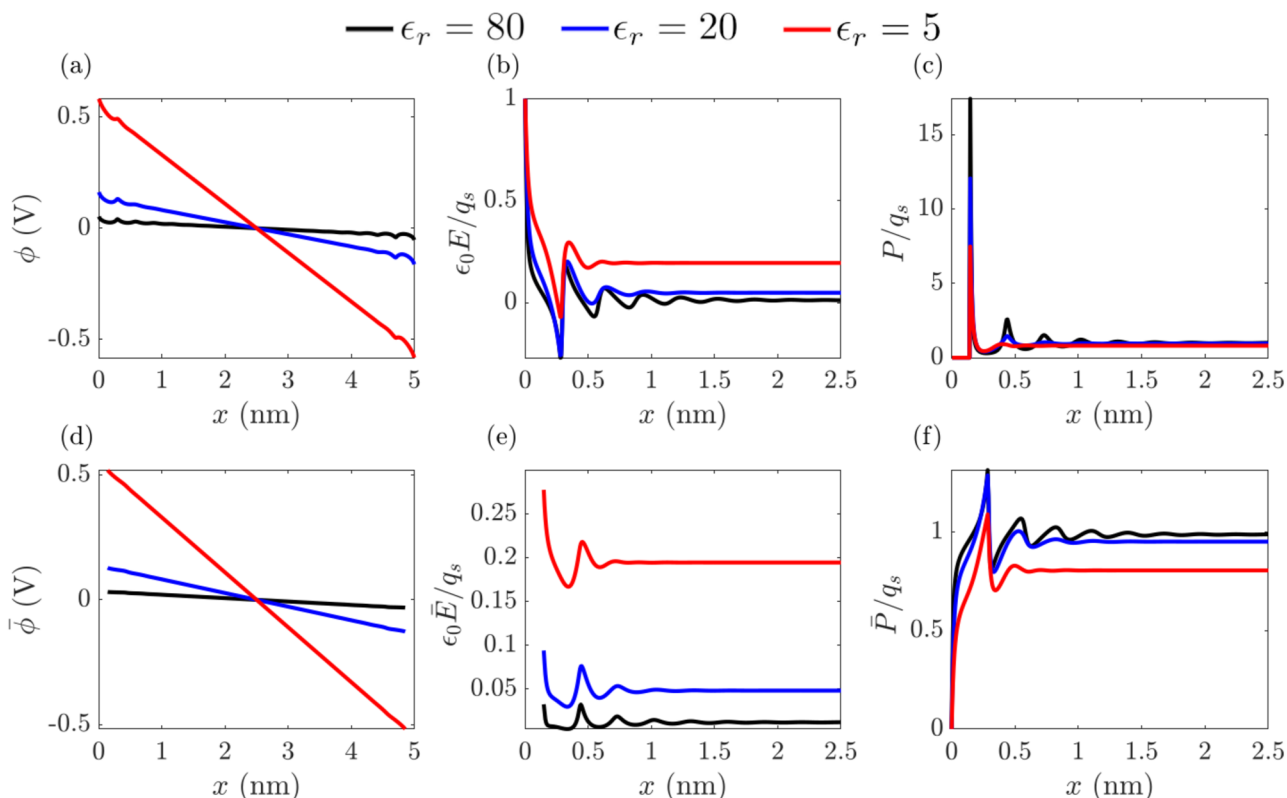


FIG. 2. Electrostatic screening by pure polar liquids between two surfaces of opposite charge shown for different values of the bulk dielectric constant, comparing the weighted and nonweighted quantities. The curves are generated by solving Eq. (24) with $\bar{\rho}_e = 0$. Variables are plotted as functions of the normal coordinate, x , zooming into the profiles emerging from the left interface for (b), (c), (e), and (f). The selected bulk dielectric permittivities correspond to the values of $\rho_0 = 4.86$ D for $\epsilon_r = 80$, $\rho_0 = 2.38$ D for $\epsilon_r = 20$, and $\rho_0 = 1.09$ D for $\epsilon_r = 5$, keeping all other parameters constant ($T = 300$ K, $L = 5$ nm, $c_{w,0} = 55$ M, $d = 0.285$ nm, and $q_s = 0.01$ C/m²). (a) Electrostatic potential, ϕ , (b) electric field, $E = -\phi'$, (c) polarization density, P , (d) weighted electrostatic potential, $\bar{\phi}$, (e) weighted electric field, $\bar{E} = -\bar{\phi}'$, and (f) weighted polarization density, \bar{P} . The local variables in (a)–(c) describe the “measured” local electrostatic response of the system, while the weighted potential and weighted electric field in (d) and (e) determine the electrochemical potential and orientation of dipoles. The weighted polarization vector in (f) corresponds to the polarization arising from the delocalized bound charge on the dipolar shells.

of the orientation of the dipoles due to the strong field intensity leads to a lower effective dielectric constant for the polar fluid in the nanoslit. Interestingly, the dipolar concentration profile at high charge density forms layers with sharp cusp-like peaks near the surface.

Finally, the behavior of the polar liquid model is studied as a function of the extent of confinement, as shown in Fig. 5. Here, the distance between the two surfaces, L , is varied between $L = 0.36$ nm to $L = 1.08$ nm. The layering in the orientation of dipole molecules relative to the normal axis, $\langle \cos(\theta) \rangle$, is complicated by the coherency of the layers of charge emanating from each surface. In the orientation profiles, we see that the spacing and number of peaks changes non-monotonically as the separation distance increases. This means that single angstrom differences in separation can lead to constructive or destructive interference from opposing layers of dipoles, forming dipolar patterns with varying orientations, periodicity, and number of layers.

B. What changes in the presence of a strong electrolyte

Commonly, dissolved ions are present in polar fluids due to the dissociation of electrolytes. In this section, we examine the screening of charge at interfaces for a polar fluid with nonzero ion concentration. Due to the nonzero ion concentration, the surface charges need not be equal nor do they need to be opposite since, as directly specified by the boundary conditions, any net charge of the two surfaces will be screened by ionic charges in the nanoslit. In nanoslits of finite lateral size in the y and z dimensions, screening charges may also exist outside the nanoslit, but this effect is not captured in our 1D model. For the purposes of this section, however, to stay in line with the pure polar fluid case, we maintain equal but opposite surface charge densities on the bounding walls of the nanoslit.

In Fig. 6, we highlight the main electrostatic properties for a 1:1 electrolyte of varying ionic concentration, c_0 . Examining the potential, ϕ , in Fig. 6(a), the overscreening oscillations seem to

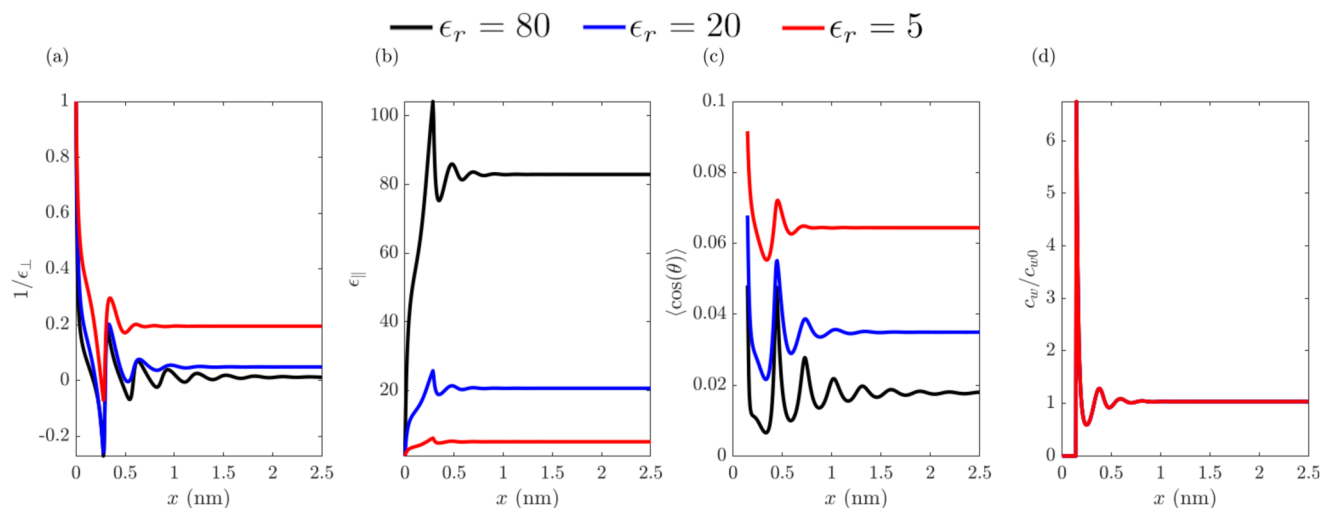


FIG. 3. Dielectric tensor, average orientation, and density of pure polar fluids between two surfaces of opposite charge, generated for model polar liquids with different values of the bulk dielectric constant. The curves are generated by solving Eq. (24) with $\bar{\rho}_e = 0$. Variables are plotted as functions of the normal coordinate, x , zooming into the profiles emerging from the left interface. The results are plotted for three pure polar fluids, corresponding to $p_0 = 4.86$ D for $\epsilon_r = 80$, $p_0 = 2.38$ D for $\epsilon_r = 20$, and $p_0 = 1.09$ D for $\epsilon_r = 5$, keeping all other parameters constant ($T = 300$ K, $L = 5$ nm, $c_{w0} = 55$ M, $d = 0.285$ nm, and $q_s = 0.01$ C/m²). (a) Normal component of the effective dielectric tensor, ϵ_{\perp} , plotted in terms of its inverse. (b) Tangential component of the effective dielectric tensor, ϵ_{\parallel} . (c) Average orientation of dipolar molecules, $\langle \cos(\theta) \rangle$. (d) Density profile of dipolar molecules, c_w , normalized by the bulk value. In (d), the density profiles are closely overlapping each other due to the low applied surface charge.

only weakly depend on the ionic concentration. The difference in the local concentrations of anions and cations, $c_- - c_+$, includes oscillatory structures for all concentrations owing to the dielectric overscreening. Furthermore, at the highest concentration, the ions themselves also contribute to overscreening, where the local ionic charge density oscillates between negative and positive values. While

the ionic concentration has a weak influence on the tangential dielectric permittivity, it strongly influences the normal component of the effective solvent dielectric permittivity. The nonzero ionic concentrations lead to longer range oscillations and more singularities in the normal component of the effective dielectric permittivity of the solvent, ϵ_{\perp} . For the highest concentration, the apparent

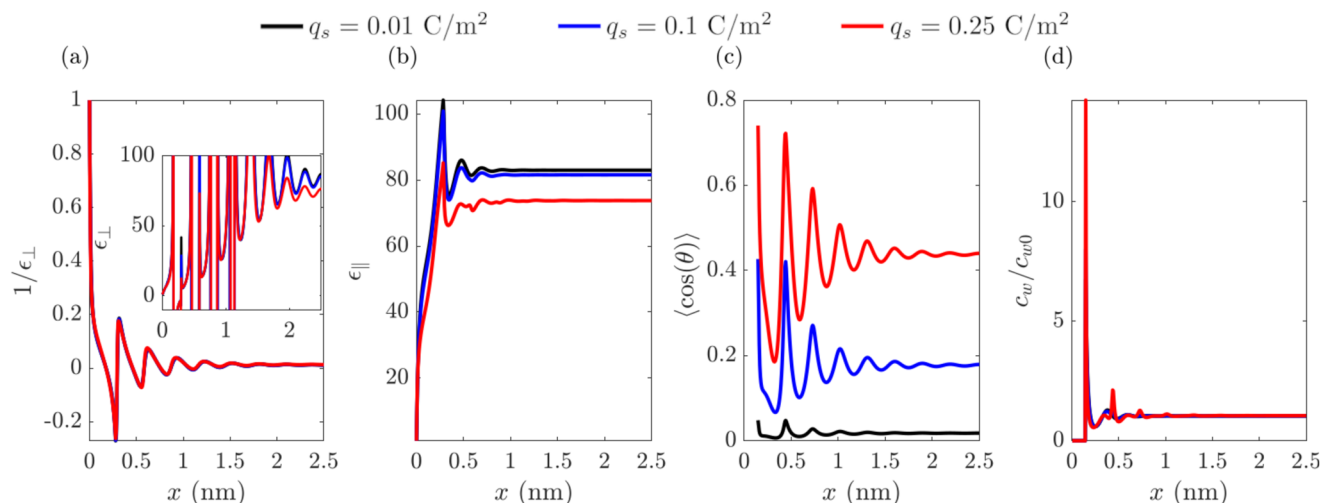


FIG. 4. Dielectric tensor, average orientation, and density of pure polar fluids between two surfaces of opposite charge for varying surface charge density. The curves are generated by solving Eq. (24) with $\bar{\rho}_e = 0$. Variables are plotted as functions of the normal coordinate, x , zooming into the profiles emerging from the left interface. The results are plotted for varying surface charge density ($q_s = 0.01$ C/m², $q_s = 0.1$ C/m², and $q_s = 0.25$ C/m²), keeping all other parameters constant ($T = 300$ K, $L = 5$ nm, $c_{w0} = 55$ M, $d = 0.285$ nm, and $p_0 = 4.86$ D). (a) Normal component of the dielectric tensor, ϵ_{\perp} , plotted in terms of its inverse. (b) Tangential component of the dielectric tensor, ϵ_{\parallel} . (c) Average orientation of dipolar molecules, $\langle \cos(\theta) \rangle$. (d) Density profile of dipolar molecules, c_w , normalized by the bulk value.

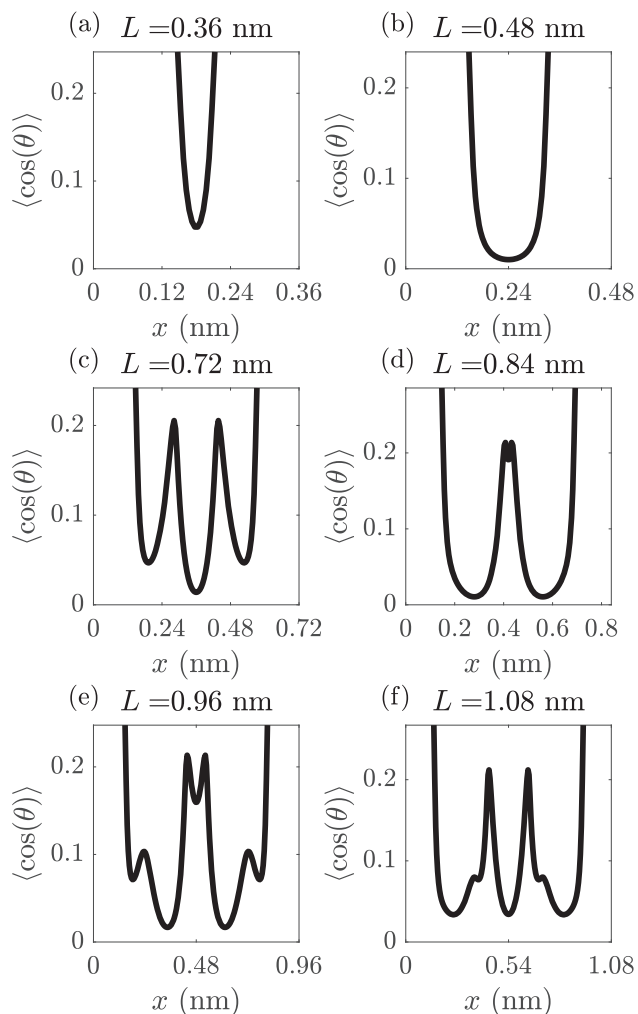


FIG. 5. Orientation of molecules in a pure polar fluid between two oppositely charged surfaces as a function of the confinement distance between the surfaces. The curves are generated by solving Eq. (24) with $\bar{\rho}_e = 0$. The results are plotted for indicated separation distances between the two confining charged surfaces, L , with (a) $L = 0.36$ nm, (b) $L = 0.48$ nm, (c) $L = 0.72$ nm, (d) $L = 0.84$ nm, (e) $L = 0.96$ nm, and (f) $L = 1.08$ nm, keeping all other parameters constant ($T = 300$ K, $c_{w0} = 55$ M, $d = 0.285$ nm, $p_0 = 4.86$ D, and $q_s = 0.05$ C/m²).

normal dielectric permittivity appears to enter an exotic region $0 < \epsilon_{\perp} < 1$, which is, of course, forbidden for the general dielectric function ϵ_{\perp}^* ,⁷⁶ but not for the effective dielectric function, ϵ_{\perp} . Note that ϵ_{\perp} is an effective quantity and the constraint of a forbidden band between 0 and 1⁷⁶ does not apply to it. The general dielectric function, ϵ_{\perp}^* , includes both the polarization of the dipoles and the polarization from ions. For our geometry, it is defined by

$$\frac{d}{dx} \left(\epsilon_0 \epsilon_{\perp}^* \frac{d\phi}{dx} \right) = 0, \quad (33)$$

and is forbidden from the region $0 < \epsilon_{\perp}^* < 1$ by the stability requirement. Here, we plot both ϵ_{\perp} [Fig. 6(c)] that satisfies Eq. (29) and ϵ_{\perp}^* [Fig. 6(e)] that satisfies Eq. (33). The general dielectric function

is computed by solving Eq. (24) and then combining the dipolar and ionic charge contributions into the ϵ_{\perp}^* function, as discussed in Appendix B. Therefore, the weighted ionic charge density acts as a source that allows for the effective solvent normal dielectric tensor component ϵ_{\perp} to enter the region $0 < \epsilon_{\perp} < 1$ when ionic overscreening occurs at high ionic concentration.

Next, the role of surface charge density on the accumulation of ions and dipolar molecules is investigated. Figure 7 shows the anion, cation, and dipolar molecule density rescaled to their bulk values ($c_0 = 0.1$ M for the ions and $c_{w0} = 55$ M for the dipoles) as the surface charge density is varied from $q_s = 0.01$ C/m² to $q_s = 0.25$ C/m². While the interfacial dipole concentration is increased at large electric field magnitudes, (the effect known under the name of ‘electrostriction’) the counterion concentration increases much more rapidly with increasing surface charge density, relative to the bulk concentration. This is quite natural as electrostriction in dense polar liquids in the electric field of the electrical double layer is a much weaker effect than the compression of the double layer with the increased voltage drop across it. Therefore, large surface potentials preferentially accumulate counterions instead of the dipolar molecules. However, when the voltage drop is large, overcrowding of counterions can occur, where layers rich in counterions of the same sign form near each of the two surfaces, pushing out the dipolar molecules further from the surface. Clearly, this conclusion depends on the size of ions and of dipoles. In the case studied here, they are of the same size. However, had this been different, for example, for a situation where the dipoles are much smaller than the ions, then the dipoles will be drawn into the double layer to screen the repulsions between the counterions.

C. Hydration forces

The layering of charged dipolar molecules confined between two interfaces causes an oscillatory hydration interaction. The hydration interaction is critical in colloidal stability, including describing forces experienced by charged biological proteins, lipid bilayers, or DNA at the nanometer scale. Here, we show that the dipolar shell theory can capture the oscillatory hydration forces commonly observed in the measurements of the forces between smooth surfaces separated by liquid films.

To calculate the disjoining pressure, we can solve the system of equations based on the electrostatic energy in Eq. (6) that is consistent with the modified Poisson equation in Eq. (24) for varied surface separation distances. The disjoining pressure calculation involves computing the overall grand potential for a given separation distance and then computing the difference in grand potential as the separation distance changes. For simpler computations, we can use the general expression for the electrostatic free energy

$$\mathcal{F}^{\text{el}}[\phi] = \int d\mathbf{r} \left\{ \frac{\epsilon_0}{2} (\nabla\phi)^2 \right\}, \quad (34)$$

and the forms of \mathcal{F}^{id} and \mathcal{F}^{ex} in Eqs. (2) and (4) to compute the overall free energy as a function of the separation distance between two surfaces. Using the above general form of the electrostatic free energy density allows us to do the free energy calculation without specific consideration of surface terms. In the calculation, we assume free exchange with a bulk reservoir at fixed concentration, the grand canonical ensemble. The grand potential can be written as

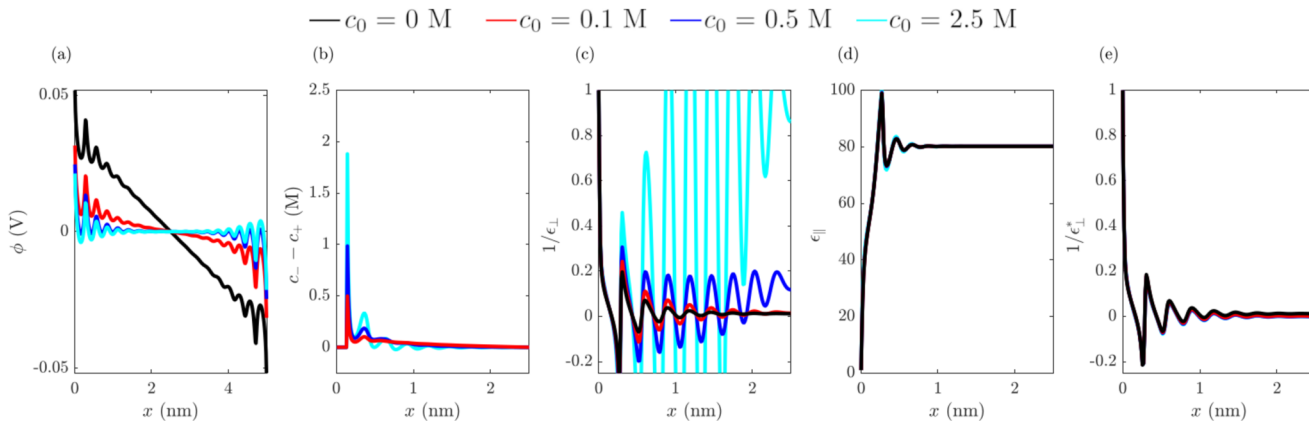


FIG. 6. Electrolyte screening behavior between two surfaces of opposite charge for varying ionic concentration. The curves are generated by solving Eq. (24) with $\bar{\rho}_e \neq 0$. The ionic concentration is varied between $c_0 = 0\text{M}$, $c_0 = 0.1\text{M}$, $c_0 = 0.5\text{M}$, and $c_0 = 2.5\text{M}$, keeping all other parameters constant ($T = 300\text{K}$, $L = 5\text{nm}$, $c_{w0} = 55\text{M}$, $d = 0.285\text{nm}$, $q_s = 0.01\text{C/m}^2$, and $\rho_0 = 4.86\text{D}$). (a) Electrostatic potential, ϕ . (b) Local difference in ionic concentration, proportional to the local charge density. (c) Normal component of the effective dielectric tensor (accounting only for the polarization of solvent), ϵ_{\perp} , plotted in terms of its inverse. (d) Tangential component of the effective dielectric tensor, ϵ_{\parallel} . (e) Normal component of the general dielectric tensor, ϵ_{\perp}^* (accounting for the polarization of the solvent and ions).

$$\Omega = \mathcal{F} - \sum_i \int d\mathbf{r} \{ \mu_{ib} c_i \}, \quad (35)$$

where $\mu_{ib} = \delta\mathcal{F}/\delta c_i|_b$. The disjoining pressure can be calculated using the relation

$$P_d = - \frac{d(\Omega/A)}{dL} \quad (36)$$

at constant temperature and reference chemical potential, where A is the area of the surfaces.^{77–80} Here, we numerically compute the integrals that define Ω/A at various values of L and numerically take the derivative to arrive at the pressure. Pressures are reported relative to the bulk reference value as $L \rightarrow \infty$, P_{∞} .

In Fig. 8, the disjoining pressure is plotted for (a) a pure polar fluid between two surfaces of opposite charge, (b) a 0.1M 1:1 electrolyte between two surfaces of opposite charge, and (c) a 0.1M 1:1 electrolyte between two surfaces of the same charge. First, we will discuss case (a) of the pure polar fluid. At zero surface charge density, the interactions are dominated by the packing effects captured in $\bar{\mu}_i^{\text{ex}}$. At larger charge density, such as $q_s = 0.30\text{C/m}^2$, the electrostatic contribution to the disjoining pressure dominates the interaction. While the initial few layers of the profile are jagged, the pressure profile gives way to regularly shaped decaying oscillations at larger separation distances. For case (b), adding in an electrolyte at low concentration ($c_0 = 0.1\text{M}$) relative to the dipole concentration ($c_{w0} = 55\text{M}$) does not significantly change the observed patterns in the short range hydration interaction at low or high surface charge

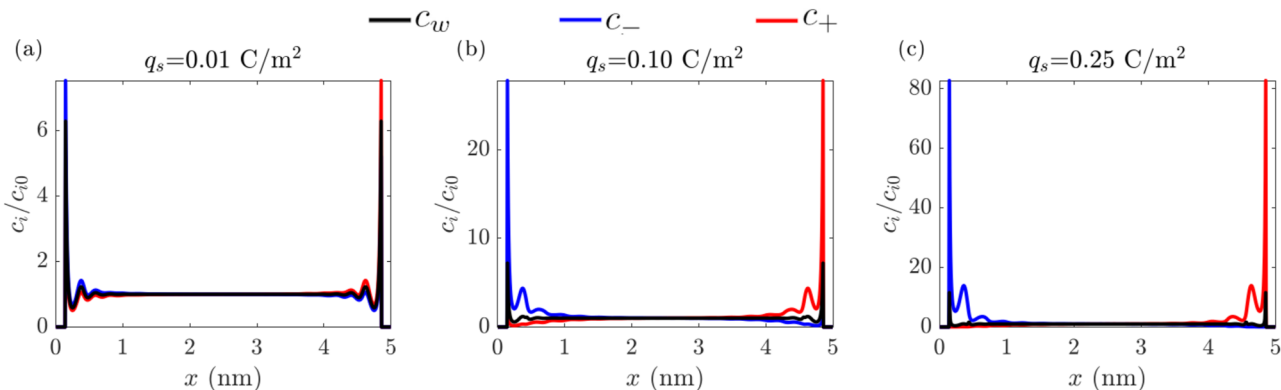


FIG. 7. Electrolyte screening behavior between two surfaces of opposite charge for varying surface charge density. The curves are generated by solving Eq. (24) with $\bar{\rho}_e \neq 0$. The surface charge density is varied between (a) $q_s = 0.01\text{C/m}^2$, (b) $q_s = 0.1\text{C/m}^2$, and (c) $q_s = 0.25\text{C/m}^2$, keeping all other parameters constant ($T = 300\text{K}$, $L = 5\text{nm}$, $c_{w0} = 55\text{M}$, $d = 0.285\text{nm}$, $c_0 = 0.1\text{M}$, and $\rho_0 = 4.86\text{D}$). The cation (red), anion (blue), and dipolar molecule (black) profiles are plotted, normalized to their respective bulk values.

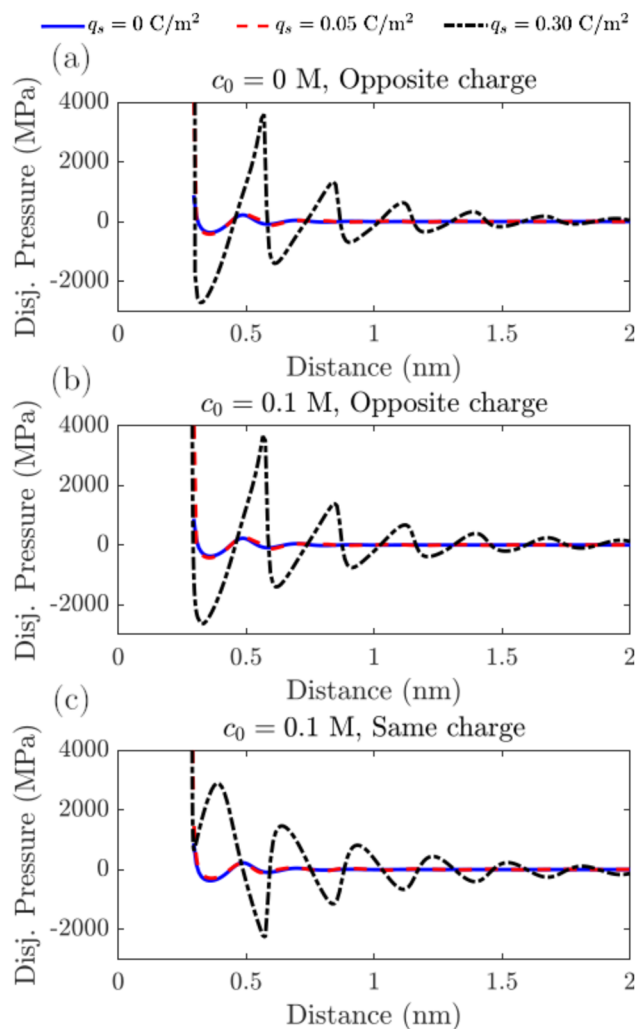


FIG. 8. The disjoining pressure between two surfaces of varying separation distance plotted for different ionic concentrations and polarity of surface charges. Individual curves correspond to the indicated surface charge density, held constant for all separation distances. The ionic concentration, c_0 , and the polarity of the surfaces are listed above each plot, indicating (a) zero ion concentration and opposite charge, (b) $c_0 = 0.1\text{ M}$ and opposite charge, and (c) $c_0 = 0.1\text{ M}$ and same charge. The three lines in each plot correspond to the values of the surface charge density from $q_s = 0, 0.05, \text{ and } 0.30\text{ C/m}^2$.

density. However, if as shown in case (c), the charge on the two surfaces is of the same sign, then the oscillation pattern is shifted and the sharpness in the patterns is flipped. Even so, the general pattern for interactions between surfaces of the same charge and of opposite charge is relatively similar in their overall envelope and long-range decay. Such an angled pressure profile dependent on the surface charge polarity, while not immediately discernible in surface force apparatus (SFA) measurements in the literature, could be detected with a carefully designed experiment if it is, in fact, present. Furthermore, measurements with soft surfaces or surfaces that are rough might blur these predicted features.

D. Model applied to double layer capacitance

In electrochemistry, one of the important measurable interfacial quantities is the double layer capacitance. In traditional theoretical approaches, the capacitance is composed of a constant Stern capacitance, C_s , and a Gouy–Chapman diffuse layer capacitance C_D in series. The Stern capacitance is assumed to arise due to the layer of water hydrating the interface with depressed dielectric constant and fixed thickness. The diffuse layer capacitance accounts for the screening of the surface charge by the ionic charge distribution in the solution near the interface. The total differential capacitance of an electrode, C_T , is defined as

$$C_T = \left| \frac{dq_s}{d\phi_s} \right|, \quad (37)$$

where ϕ_s is the surface potential. The total differential capacitance is, therefore, related to the Stern and Debye capacitance,

$$C_T = (C_D^{-1} + C_s^{-1})^{-1}. \quad (38)$$

At small potential drops across the double layer for dilute solutions, the diffuse layer capacitance is approximately equal to the Debye capacitance,

$$C_D = \frac{\epsilon_r \epsilon_0}{\lambda_D}, \quad (39)$$

where λ_D is the Debye length,

$$\lambda_D = \sqrt{\frac{\epsilon_r \epsilon_0 k_B T}{2e^2 c_0}}. \quad (40)$$

In the dipolar shell theory, the equally sized hard sphere assumption means that there is no layer of water near the surface. In the model, the water layering and ionic screening occur in a diffuse manner from the interface. Despite the overlap, the layering of water still leads to an *effective* Stern capacitance.¹⁵

In Fig. 9, we calculate the variation in the total double layer capacitance, effective Stern capacitance, and calculated Debye capacitance as the ionic concentration changes, all calculated near the point of zero charge for non-overlapping double layers. While the theory does not contain a specific layer of water at an interface like the traditional Stern layer concept, it returns a nearly constant effective Stern capacitance around $60\text{ }\mu\text{F/cm}^2$. The general predictions of semi-phenomenological nonlocal electrostatic theory in Refs. 15–17 are fully supported by this “molecular” level model. The details of the capacitance could be affected strongly by the size asymmetry of real polar liquids and ions. In other words, small water molecules would access the surface more easily than larger ions in the solution in order to reduce the electrostatic repulsion between the counterions. Furthermore, the induced polarization of the solvent and ions can strongly affect the capacitance.⁸¹

E. Linearized form of equations

The system of equations outlined above are generally nonlinear integro-differential equations. While they can be solved in a straightforward manner numerically, they do not admit simple analytical solutions. Here, we show how the system of equations can be reduced to linear differential forms, where the oscillatory decay can

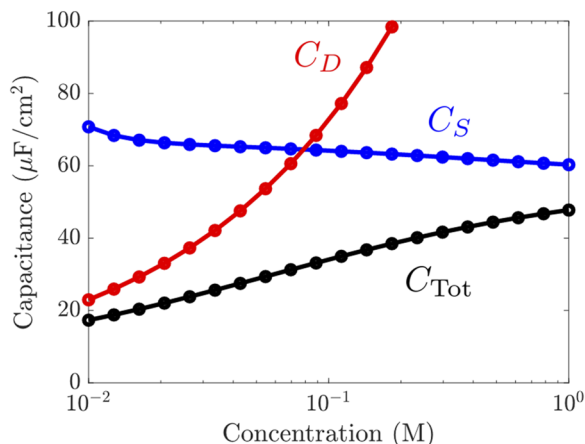


FIG. 9. Effective capacitance at zero charge for an electrolyte as a function of ionic concentration. All other parameters are kept constant ($T = 300$ K, $L = 5$ nm, $c_{w0} = 55$ M, $d = 0.285$ nm, and $\rho_0 = 4.86$ D). The total capacitance is calculated numerically from an isolated double layer. The Debye capacitance is calculated as $C_D = \epsilon_r \epsilon_0 / \lambda_D$, and the effective Stern capacitance is calculated assuming a series capacitance model to match the total capacitance from the dipolar shell theory.

be described analytically. While not valid for the first few layers of oscillations in charge and mass, the linearized forms of the theory are decent approximations for the long-range behavior of the polar fluid.

The linearized weighted Langevin–Poisson equation for the dipolar shell theory [combining linearized forms of Eqs. (17), (20) and (21)] is

$$\left[1 + (\epsilon_r - 1)\hat{w}_s^2\right]\nabla^2\phi = \epsilon_r\kappa_D^2\hat{w}_s^2\phi, \quad (41)$$

where κ_D is the inverse Debye length and ϕ is written in its local form. For small perturbations, we can assume that the convolution with w_s acts as a differential operator, $\hat{w}_s \approx 1 + \ell_s^2 \nabla^2$, where $\ell_s = d/\sqrt{24}$.⁵⁹ The $\hat{\cdot}$ symbol corresponds to the differential form of the weighting function. In 1D, if we assume $\phi = A \exp(\kappa x)$, we get the following characteristic equation for the decaying modes:

$$\kappa^2 + (1 + \kappa^2 \ell_s^2)^2 [(\epsilon_r - 1)\kappa^2 - \epsilon_r \kappa_D^2] = 0. \quad (42)$$

If there is no electrolyte present, $\kappa_D = 0$, then the solution for κ has a real and imaginary parts as

$$\begin{aligned} \text{Re}(\kappa) &= 0, \quad \pm \frac{1}{\ell_s} \sqrt{-\frac{1}{2} + \frac{1}{2} \sqrt{\frac{\epsilon_r}{\epsilon_r - 1}}}, \\ \text{Im}(\kappa) &= 0, \quad \pm \frac{1}{\ell_s} \sqrt{\frac{1}{2} + \frac{1}{2} \sqrt{\frac{\epsilon_r}{\epsilon_r - 1}}}. \end{aligned} \quad (43)$$

The zero solutions correspond to a linear potential profile, while the superimposed nonzero solutions correspond to the structuring of the liquid at the interface. The real part describes the exponential decay of oscillations, with the sign chosen to give eventual decay

into the bulk. The imaginary part gives information on the period of oscillations. In the limit of large $(\epsilon_r - 1)$, we get

$$\begin{aligned} \text{Re}(\kappa) &= 0, \quad \pm \frac{1}{2\ell_s \sqrt{\epsilon_r - 1}}, \\ \text{Im}(\kappa) &= 0, \quad \pm \frac{1}{\ell_s}. \end{aligned} \quad (44)$$

This means that in the absence of ions, the effective hydration length governing decay of the oscillations scales as

$$\lambda_s = d\sqrt{(\epsilon_r - 1)/6}, \quad (45)$$

and an oscillation wavelength of about one molecular diameter. For water, the effective hydration length turns out to be ≈ 1 nm at room temperature. The hydration length describes the decay of the alternating layers of bound charge emanating from a surface, and the magnitude of this decaying mode is determined by the magnitude of polarization at the surface.

Now, if we include salt, the expressions for the decaying modes become more complicated. In the limit of small but non-zero ion concentrations, $\kappa_D \rightarrow 0$ gives a longest decaying mode of $\kappa = \kappa_D$, where the effective decay length is the Debye length, λ_D . In this limit, the hydration length can be thought to be independent of and additive to the long range Debye screening, as is commonly assumed in experimental measurements of surface forces.⁴³

In the limit of large ionic concentrations and large $(\epsilon_r - 1)$, another simplified formula can be attained for the slowest decaying mode,

$$\kappa \approx \frac{1}{2\sqrt{\epsilon_r}\kappa_D\ell_s^2} \pm \frac{i}{\ell_s}. \quad (46)$$

This formula is valid when $\sqrt{\epsilon_r}\kappa_D\ell_s \gg 1$, meaning that the molecule size is much larger than the Debye length in vacuum. The effective screening length becomes independent of the relative permittivity,

$$\lambda_s \approx \frac{2\ell_s^2\sqrt{\epsilon_r}}{\lambda_D} = \frac{d^2\sqrt{\epsilon_r}}{12\lambda_D}, \quad (47)$$

since the dependence of ϵ_r cancels out [c.f. Eq. (40)], and the oscillations are on the order of one molecular diameter.

An additional source of oscillations is from the density variations owing to packing of molecules at a flat interface. Taking each set of species, we can assume small perturbations,

$$\begin{aligned} c_w &\approx c_{w0}(1 - \beta\bar{\mu}^{\text{ex}}), \\ c_i &\approx c_{i0}(1 - z_i e\beta\bar{\phi} - \beta\bar{\mu}^{\text{ex}}). \end{aligned} \quad (48)$$

If we sum over all species assuming the same size of each molecule and, thus, identical excess chemical potential, we get an expression for the local filling fraction,

$$\eta - \eta_0 = -\eta_0\beta\bar{\mu}^{\text{ex}} = -\frac{2\eta_0(4 - \eta_0)}{(\eta_0 - 1)^4} \hat{w}_v^2(\eta - \eta_0), \quad (49)$$

where we have linearized the excess chemical potential. We can again assume small perturbations and treat w_v as an operator, $\hat{w}_v \approx 1 + \ell_v^2 \nabla^2$, where $\ell_v = d/\sqrt{40}$. The decay of the density for

a symmetric fluid is independent of the decay of the electrostatic potential, and the characteristic equation, assuming $\eta - \eta_0 = A \exp(-\kappa_m x)$, is given by

$$1 + \frac{2\eta_0(4 - \eta_0)}{(\eta_0 - 1)^4} (1 + \ell_v^2 \kappa_m^2)^2 = 0. \quad (50)$$

Here, κ_m has real and imaginary parts,

$$\begin{aligned} \operatorname{Re}(\kappa_m) &= \frac{1}{\ell_v} \sqrt{-\frac{1}{2} + \frac{1}{2} \sqrt{1 + \frac{(1 - \eta_0)^4}{2\eta_0(4 - \eta_0)}}}, \\ \operatorname{Im}(\kappa_m) &= \frac{1}{\ell_v} \sqrt{\frac{1}{2} + \frac{1}{2} \sqrt{1 + \frac{(1 - \eta_0)^4}{2\eta_0(4 - \eta_0)}}}. \end{aligned} \quad (51)$$

As $\eta_0 \rightarrow 0$, the oscillations decay rapidly over a small length scale $\lambda_m = \ell_v (8\eta_0)^{1/4}$. For dense solutions, as $\eta_0 \rightarrow 1$, the real and imaginary parts of the solution result in

$$\begin{aligned} \operatorname{Re}(\kappa_m) &= \frac{(1 - \eta_0)^2}{\sqrt{8\ell_v} \sqrt{\eta_0(4 - \eta_0)}}, \\ \operatorname{Im}(\kappa_m) &= \frac{1}{\ell_v}. \end{aligned} \quad (52)$$

In other words, the decay of mass oscillations with the wavelength of the molecular diameter goes as

$$\lambda_m \approx \sqrt{\frac{1}{5}} \frac{d\sqrt{\eta_0(4 - \eta_0)}}{(1 - \eta_0)^2}. \quad (53)$$

For water at room temperature, the decay length for mass oscillations is $\lambda_m \approx 0.4$ nm. Therefore, the mass density oscillations decay more rapidly (over a shorter length scale) than the oscillations in the potential. While the typical filling fraction for pure liquids is around $\eta_0 \approx 0.4$, an increase in the filling fraction corresponds to longer range oscillations in the liquid number density. As $\eta_0 \rightarrow 1$, the predicted decay length tends to infinity, corresponding to a crystal. At extremely high filling fractions, the Carnahan-Starling equation of state may not be appropriate near the jamming limit. Regardless, the usual bulk filling fraction of typical liquids is much smaller than one. The competition between mass and hydration length depends on the filling fraction of the fluid and the relative dielectric constant of the fluid, as well as the magnitude of the surface charge density or surface potential. Even so, the oscillation wavelength for electrostatics and density variations remains comparable to the molecular or ionic diameter for each decay mode.

Thus, for highly charged surfaces, we expect to see oscillation patterns with the period of oscillations of the liquid molecule size and decay envelope of the order of 1 nm determined by the hydration length in Eq. (45), whereas for low charged or uncharged surfaces, the envelope will be much shorter based on Eq. (53). In experiments, people saw a variance of decay length of the force between neutral surfaces,⁸² but this was explained by lateral inhomogeneity of the generally electroneutral charge distribution along the surface.⁸³ The oscillations themselves get smeared by the smearing of the surfaces. Our model suggests that the interplay of charge ordering and packing effects will influence the observed decaying modes, as was demonstrated clearly by

studying the hydration forces in Fig. 8 with varying surface charge magnitudes.

IV. CONCLUSIONS

The dipolar shell theory describes layering in charge and mass for an interfacial polar fluid. In this work, we have demonstrated that the effective delocalized bound charge on the dipolar molecules underlies the overscreening phenomenon, with alternating layers of bound charge density on the dipoles.

The overscreening effect leads to significant anisotropy in the normal and tangential components of the permittivity. The normal component has singularities owing to the overscreening effect, while the tangential component scales more closely with the dipole concentration. The length scale governing the decay of oscillations from the interface is the *hydration length*, $\lambda_s = d\sqrt{(\epsilon_r - 1)/6}$.

When ions are present, the ionic layering is influenced by the structuring of the polar fluid, and the ions also begin to contribute to the overscreening effect when they reach a sufficiently high concentration.

The theory could be extended further and applied to various other applications not mentioned in this work. Straightforward extensions of the theory could describe the following: (i) varying electrolyte composition with multivalent ions and mixtures of polar fluids, (ii) varying the geometry of the pore domain to cylindrical or spherical pores or using the theory to describe the double layer structure around cylindrical or spherical charged colloids, (iii) extending the analysis to non-uniform ion and water sizes, (iv) demonstrating the charging dynamics of the dipolar fluid orientation and layering, (v) showing the role of double layer and hydration oscillation overlap on the system capacitance, (vi) demonstrating the role of the dipolar fluid organization on the effective ζ -potential for electrokinetic measurements, and (vii) including the interfacial polar liquid structure in a formulation of interfacial electrochemical reactions.

Although the theory does capture the charge structuring at the interface, it still falls short of perfectly describing real polar liquids. For example, the theory does not reproduce the single-ion-level hydration. A more sophisticated approach may be necessary to keep track of the bound and free states of water that constitute the coordinated hydration shell of individual ions. Furthermore, the theory only indirectly captures the correlations between neighboring dipolar molecules, which requires an effective dipole moment that is larger than the true value for highly polar fluids.

The dipolar shell structure assumed in the theory is significantly simpler than typical charge distributions within polar molecules. For example, the higher-order multipole moments of water can strongly influence the interfacial polarization.^{35,84,85} The model assumes a hard sphere repulsion, but real polar fluids will have softer repulsive interactions, as well as attractive dispersion interactions. Finally, we have neglected electronic degrees of freedom, always present in polar fluids, which contribute to the dielectric constant of the liquid independent of the fixed dipole orientations.

Despite the simplifications, the dipolar shell theory presents a powerful theoretical framework to investigate the interfacial properties of polar liquids. The system of integro-differential equations is readily soluble, especially in 1D geometries. The approximate, differential form of the theory gives analytical formulas for quick estimates and experimental comparisons.

ACKNOWLEDGMENTS

All the authors acknowledge the support from the MIT-Imperial College Seed Fund. J.P.D. and M.Z.B. acknowledge the support from the Center for Enhanced Nanofluidic Transport, an Energy Frontier Research Center funded by the U.S. Department of Energy, Office of Science, Basic Energy Sciences, under Award No. DE-SC0019112. J.P.D. also acknowledges funding from the National Science Foundation Graduate Research Fellowship under Award Number No. 1122374. A.A.K. would like to acknowledge the research grant by the Leverhulme Trust (Grant No. RPG-2016-223). The authors thank Karina Pivnic, Aditya Limaye, and Michael Urbakh for useful discussions.

AUTHOR DECLARATIONS

Conflict of Interest

The authors have no conflicts to disclose.

Author Contributions

J. Pedro de Souza: Conceptualization (lead); Formal analysis (lead); Investigation (lead); Methodology (lead); Visualization (lead); Writing – original draft (lead); Writing – review & editing (lead). **Alexei A. Kornyshev:** Conceptualization (supporting); Funding acquisition (equal); Supervision (equal); Writing – original draft (supporting); Writing – review & editing (equal). **Martin Z. Bazant:** Conceptualization (supporting); Funding acquisition (lead); Project administration (lead); Resources (lead); Supervision (equal); Writing – original draft (supporting); Writing – review & editing (supporting).

DATA AVAILABILITY

The data that support the findings of this study are available from the corresponding author upon reasonable request.

APPENDIX A: DERIVATION OF ELECTROSTATIC FREE ENERGY

Here, we reduce the electrostatic free energy to the form presented in the main text. The free energy can be defined as

$$\mathcal{F}^{\text{el}}[\phi] = \int d\mathbf{r} \left\{ \frac{\epsilon_0}{2} (\nabla\phi)^2 \right\}. \quad (\text{A1})$$

The modified form of Poisson's equation can be written as

$$0 = \epsilon_0 \nabla^2 \phi + \bar{\rho}_b + \bar{\rho}_e \quad (\text{A2})$$

in terms of the weighted bound charge density or as

$$0 = \epsilon_0 \nabla^2 \phi - \nabla \cdot \bar{\mathbf{P}} + \bar{\rho}_e \quad (\text{A3})$$

in terms of the weighted polarization vector.

Here, we employ a Lagrange multiplier, λ , to enforce the modified Poisson equation in our minimization of the electrostatic free energy,

$$\mathcal{F}^{\text{el}}[\phi, \bar{\rho}_e, \bar{\mathbf{P}}, \lambda] = \int d\mathbf{r} \left\{ \frac{\epsilon_0}{2} (\nabla\phi)^2 + \lambda (\epsilon_0 \nabla^2 \phi - \nabla \cdot \bar{\mathbf{P}} + \bar{\rho}_e) \right\}. \quad (\text{A4})$$

Taking a variation with respect to ϕ , we find that $\lambda = \phi$. Plugging in this dependence gives

$$\mathcal{F}^{\text{el}}[\phi, \bar{\rho}_e, \bar{\mathbf{P}}] = \int d\mathbf{r} \left\{ \frac{\epsilon_0}{2} (\nabla\phi)^2 + \phi (\epsilon_0 \nabla^2 \phi - \nabla \cdot \bar{\mathbf{P}} + \bar{\rho}_e) \right\}. \quad (\text{A5})$$

Using the divergence theorem, we can find the following identity:

$$\begin{aligned} \phi (\epsilon_0 \nabla^2 \phi - \nabla \cdot \bar{\mathbf{P}} + \bar{\rho}_e) &= \nabla \cdot (\epsilon_0 \phi \nabla \phi) - \epsilon_0 (\nabla \phi)^2 \\ &\quad - \nabla \cdot (\phi \bar{\mathbf{P}}) + \bar{\mathbf{P}} \cdot \nabla \phi + \bar{\rho}_e \phi. \end{aligned} \quad (\text{A6})$$

Here, we can take the divergence terms to a surface far away, where the potential and related fields are zero, leaving the following expression for the electrostatic energy:

$$\mathcal{F}^{\text{el}}[\phi, \bar{\rho}_e, \bar{\mathbf{P}}] = \int d\mathbf{r} \left\{ -\frac{\epsilon_0}{2} (\nabla\phi)^2 + \bar{\rho}_e \phi + \bar{\mathbf{P}} \cdot \nabla \phi \right\}. \quad (\text{A7})$$

Equalizing to zero the variational derivative $\delta\mathcal{F}^{\text{el}}/\delta\phi$ returns the modified Poisson equation. Note that while the functional appears non-convex, the unaltered electrostatic free energy in Eq. (A1) ensures convexity of the electrostatic free energy. Therefore, any function for the potential that satisfies the modified Poisson equation is also guaranteed to minimize the electrostatic free energy within the constraints.

APPENDIX B: CALCULATION OF THE GENERAL DIELECTRIC FUNCTION

The normal component of the general dielectric tensor, ϵ_{\perp}^* , which satisfies Eq. (33), can be equated to the charge and polarization density variables by collecting terms so as to arrive at Eq. (24). ϵ_{\perp}^* can, therefore, be defined as

$$\epsilon_{\perp}^* = 1 - \frac{(\bar{\mathbf{P}} - \int_0^x \bar{\rho}_e(\xi) d\xi)}{\epsilon_0 \phi'}, \quad (\text{B1})$$

where both the bound charge density on dipoles and the ionic charge density are included. We see that the direct substitution of the above relation into Eq. (33) returns Eq. (24).

REFERENCES

- ¹M. Chaplin, "Do we underestimate the importance of water in cell biology?" *Nat. Rev. Mol. Cell Biol.* **7**, 861–866 (2006).
- ²P. Ball, "Water as an active constituent in cell biology," *Chem. Rev.* **108**, 74–108 (2008).
- ³A. J. Bard and L. R. Faulkner, *Electrochemical Methods: Fundamentals and Applications* (Wiley, New York, 2001).
- ⁴J. N. Israelachvili, *Intermolecular and Surface Forces* (Academic Press, 2011).
- ⁵J. Lyklema, *Fundamentals of Interface and Colloid Science, Solid-Liquid Interfaces* (Academic Press., 1995), Vol. 2.
- ⁶G. M. Geise, D. R. Paul, and B. D. Freeman, "Fundamental water and salt transport properties of polymeric materials," *Prog. Polym. Sci.* **39**, 1–42 (2014).

- ⁷S. Marbach and L. Bocquet, "Osmosis, from molecular insights to large-scale applications," *Chem. Soc. Rev.* **48**, 3102–3144 (2019).
- ⁸F. Bowden and D. Tabor, *The Friction and Lubrication of Solids* (Oxford University, New York, 1950).
- ⁹B. Bhushan, J. N. Israelachvili, and U. Landman, "Nanotribology: Friction, wear and lubrication at the atomic scale," *Nature* **374**, 607–616 (1995).
- ¹⁰O. Björneholm, M. H. Hansen, A. Hodgson, L.-M. Liu, D. T. Limmer, A. Michaelides, P. Pedevilla, J. Rossmeisl, H. Shen, G. Tocci *et al.*, "Water at interfaces," *Chem. Rev.* **116**, 7698–7726 (2016).
- ¹¹M. Gouy, "Sur la constitution de la charge électrique à la surface d'un électrolyte," *J. Phys. Theor. Appl.* **9**, 457–468 (1910).
- ¹²D. L. Chapman, "LI. A contribution to the theory of electrocapillarity," *London, Edinburgh Dublin Philos. Mag. J. Sci.* **25**, 475–481 (1913).
- ¹³O. Stern, "Zur theorie der elektrolytischen doppelschicht," *Z. Elektrochem. Angew. Phys. Chem.* **30**, 508–516 (1924).
- ¹⁴M. Z. Bazant, M. S. Kilic, B. D. Storey, and A. Ajdari, "Towards an understanding of induced-charge electrokinetics at large applied voltages in concentrated solutions," *Adv. Colloid Interface Sci.* **152**, 48–88 (2009).
- ¹⁵A. A. Kornyshev, W. Schmickler, and M. A. Vorotyntsev, "Nonlocal electrostatic approach to the problem of a double layer at a metal-electrolyte interface," *Phys. Rev. B* **25**, 5244 (1982).
- ¹⁶A. A. Kornyshev and M. A. Vorotyntsev, "Nonlocal electrostatic approach to the double layer and adsorption at the electrode-electrolyte interface," *Surf. Sci.* **101**, 23–48 (1980).
- ¹⁷A. A. Kornyshev and M. A. Vorotyntsev, "Nonlocal dielectric response of the electrode/solvent interface in the double layer problem," *Can. J. Chem.* **59**, 2031–2042 (1981).
- ¹⁸D. J. Bonthuis and R. R. Netz, "Beyond the continuum: How molecular solvent structure affects electrostatics and hydrodynamics at solid-electrolyte interfaces," *J. Phys. Chem. B* **117**, 11397–11413 (2013).
- ¹⁹D. C. Grahame, "Effects of dielectric saturation upon the diffuse double layer and the free energy of hydration of ions," *J. Chem. Phys.* **18**, 903–909 (1950).
- ²⁰A. Abrashkin, D. Andelman, and H. Orland, "Dipolar Poisson-Boltzmann equation: Ions and dipoles close to charge interfaces," *Phys. Rev. Lett.* **99**, 077801 (2007).
- ²¹J. N. Israelachvili and R. M. Pashley, "Molecular layering of water at surfaces and origin of repulsive hydration forces," *Nature* **306**, 249–250 (1983).
- ²²P. Fenter and N. C. Sturchio, "Mineral-water interfacial structures revealed by synchrotron x-ray scattering," *Prog. Surf. Sci.* **77**, 171–258 (2004).
- ²³L. Cheng, P. Fenter, K. L. Nagy, M. L. Schlegel, and N. C. Sturchio, "Molecular-scale density oscillations in water adjacent to a mica surface," *Phys. Rev. Lett.* **87**, 156103 (2001).
- ²⁴J. G. Catalano, "Weak interfacial water ordering on isostructural hematite and corundum (0 0 1) surfaces," *Geochim. Cosmochim. Acta* **75**, 2062–2071 (2011).
- ²⁵D. Frydel and Y. Levin, "A close look into the excluded volume effects within a double layer," *J. Chem. Phys.* **137**, 164703 (2012).
- ²⁶D. Gillespie, "A review of steric interactions of ions: Why some theories succeed and others fail to account for ion size," *Microfluid. Nanofluid.* **18**, 717–738 (2015).
- ²⁷M. Valiskó, T. Kristóf, D. Gillespie, and D. Boda, "A systematic Monte Carlo simulation study of the primitive model planar electrical double layer over an extended range of concentrations, electrode charges, cation diameters and valences," *AIP Adv.* **8**, 025320 (2018).
- ²⁸J. P. de Souza and M. Z. Bazant, "Continuum theory of electrostatic correlations at charged surfaces," *J. Phys. Chem. C* **124**, 11414–11421 (2020).
- ²⁹P. Cats, R. Evans, A. Härtel, and R. van Roij, "Primitive model electrolytes in the near and far field: Decay lengths from DFT and simulations," *J. Chem. Phys.* **154**, 124504 (2021).
- ³⁰P. A. Bopp, A. A. Kornyshev, and G. Sutmann, "Frequency and wave-vector dependent dielectric function of water: Collective modes and relaxation spectra," *J. Chem. Phys.* **109**, 1939–1958 (1998).
- ³¹P. A. Bopp, A. A. Kornyshev, and G. Sutmann, "Static nonlocal dielectric function of liquid water," *Phys. Rev. Lett.* **76**, 1280 (1996).
- ³²A. A. Kornyshev and G. Sutmann, "Nonlocal dielectric saturation in liquid water," *Phys. Rev. Lett.* **79**, 3435 (1997).
- ³³A. A. Kornyshev and G. Sutmann, "The shape of the nonlocal dielectric function of polar liquids and the implications for thermodynamic properties of electrolytes: A comparative study," *J. Chem. Phys.* **104**, 1524–1544 (1996).
- ³⁴D. J. Bonthuis, S. Gekle, and R. R. Netz, "Dielectric profile of interfacial water and its effect on double-layer capacitance," *Phys. Rev. Lett.* **107**, 166102 (2011).
- ³⁵D. J. Bonthuis, S. Gekle, and R. R. Netz, "Profile of the static permittivity tensor of water at interfaces: Consequences for capacitance, hydration interaction and ion adsorption," *Langmuir* **28**, 7679–7694 (2012).
- ³⁶A. Schlaich, E. W. Knapp, and R. R. Netz, "Water dielectric effects in planar confinement," *Phys. Rev. Lett.* **117**, 048001 (2016).
- ³⁷P. Loche, C. Ayaz, A. Schlaich, D. J. Bonthuis, and R. R. Netz, "Breakdown of linear dielectric theory for the interaction between hydrated ions and graphene," *J. Phys. Chem. Lett.* **9**, 6463–6468 (2018).
- ³⁸S. Ruiz-Barragan, D. Muñoz-Santiburcio, S. Körning, and D. Marx, "Quantifying anisotropic dielectric response properties of nanoconfined water within graphene slit pores," *Phys. Chem. Chem. Phys.* **22**, 10833–10837 (2020).
- ³⁹A. Levy, D. Andelman, and H. Orland, "Dielectric constant of ionic solutions: A field-theory approach," *Phys. Rev. Lett.* **108**, 227801 (2012).
- ⁴⁰A. Iglič, E. Gongadze, and K. Bohinc, "Excluded volume effect and orientational ordering near charged surface in solution of ions and Langevin dipoles," *Bioelectrochemistry* **79**, 223–227 (2010).
- ⁴¹R. Prasanna Misra, S. Das, and S. K. Mitra, "Electric double layer force between charged surfaces: Effect of solvent polarization," *J. Chem. Phys.* **138**, 114703 (2013).
- ⁴²M. McEldrew, Z. A. H. Goodwin, A. A. Kornyshev, and M. Z. Bazant, "Theory of the double layer in water-in-salt electrolytes," *J. Phys. Chem. Lett.* **9**, 5840–5846 (2018).
- ⁴³A. A. Kornyshev, "Non-local dielectric response of a polar solvent and Debye screening in ionic solution," *J. Chem. Soc., Faraday Trans. 2* **79**, 651–661 (1983).
- ⁴⁴M. L. Belaya, M. V. Feigel'man, and V. G. Levadny, "Hydration forces as a result of non-local water polarizability," *Chem. Phys. Lett.* **126**, 361–364 (1986).
- ⁴⁵A. Levy, M. Bazant, and A. Kornyshev, "Ionic activity in concentrated electrolytes: Solvent structure effect revisited," *Chem. Phys. Lett.* **738**, 136915 (2020).
- ⁴⁶R. Blossey, A. C. Maggs, and R. Podgornik, "Structural interactions in ionic liquids linked to higher-order Poisson-Boltzmann equations," *Phys. Rev. E* **95**, 060602 (2017).
- ⁴⁷D. Chandler and H. C. Andersen, "Optimized cluster expansions for classical fluids. II. Theory of molecular liquids," *J. Chem. Phys.* **57**, 1930–1937 (1972).
- ⁴⁸F. Hirata, B. M. Pettitt, and P. J. Rossky, "Application of an extended RISM equation to dipolar and quadrupolar fluids," *J. Chem. Phys.* **77**, 509–520 (1982).
- ⁴⁹B. M. Pettitt and P. J. Rossky, "Integral equation predictions of liquid state structure for waterlike intermolecular potentials," *J. Chem. Phys.* **77**, 1451–1457 (1982).
- ⁵⁰M. Ikeguchi and J. Doi, "Direct numerical solution of the Ornstein-Zernike integral equation and spatial distribution of water around hydrophobic molecules," *J. Chem. Phys.* **103**, 5011–5017 (1995).
- ⁵¹L. Lue and D. Blankschtein, "Application of integral equation theories to predict the structure, thermodynamics, and phase behavior of water," *J. Chem. Phys.* **102**, 5427–5437 (1995).
- ⁵²D. Beglov and B. Roux, "An integral equation to describe the solvation of polar molecules in liquid water," *J. Phys. Chem. B* **101**, 7821–7826 (1997).
- ⁵³A. Trokhymchuk, D. Henderson, and D. T. Wasan, "A molecular theory of the hydration force in an electrolyte solution," *J. Colloid Interface Sci.* **210**, 320–331 (1999).
- ⁵⁴Q. Du, D. Beglov, and B. Roux, "Solvation free energy of polar and nonpolar molecules in water: An extended interaction site integral equation theory in three dimensions," *J. Phys. Chem. B* **104**, 796–805 (2000).
- ⁵⁵M. V. Fedorov and A. A. Kornyshev, "Unravelling the solvent response to neutral and charged solutes," *Mol. Phys.* **105**, 1–16 (2007).
- ⁵⁶J. Wu and Z. Li, "Density-functional theory for complex fluids," *Annu. Rev. Phys. Chem.* **58**, 85–112 (2007).
- ⁵⁷J.-F. Olivieri, J. T. Hynes, and D. Laage, "Confined water's dielectric constant reduction is due to the surrounding low dielectric media and not to interfacial molecular ordering," *J. Phys. Chem. Lett.* **12**, 4319–4326 (2021).

- ⁵⁸F. Deisenbeck, C. Freysoldt, M. Todorova, J. Neugebauer, and S. Wippermann, "Dielectric properties of nanoconfined water: A canonical thermopotential approach," *Phys. Rev. Lett.* **126**, 136803 (2021).
- ⁵⁹J. P. de Souza, Z. A. H. Goodwin, M. McEldrew, A. A. Kornyshev, and M. Z. Bazant, "Interfacial layering in the electric double layer of ionic liquids," *Phys. Rev. Lett.* **125**, 116001 (2020).
- ⁶⁰D. Frydel and Y. Levin, "The double-layer of penetrable ions: An alternative route to charge reversal," *J. Chem. Phys.* **138**, 174901 (2013).
- ⁶¹Z. G. Wang, "Fluctuation in electrolyte solutions: The self energy," *Phys. Rev. E* **81**, 021501 (2010).
- ⁶²S. May, A. Iglič, J. Reščič, S. Maset, and K. Bohinc, "Bridging like-charged macroions through long divalent rodlike ions," *J. Phys. Chem. B* **112**, 1685–1692 (2008).
- ⁶³D. Frydel, "Mean-field electrostatics beyond the point-charge description," *Adv. Chem. Phys.* **160**, 209–260 (2016).
- ⁶⁴D. Frydel, "The double-layer structure of overscreened surfaces by smeared-out ions," *J. Chem. Phys.* **145**, 184703 (2016).
- ⁶⁵R. M. Adar, S. A. Safran, H. Diamant, and D. Andelman, "Screening length for finite-size ions in concentrated electrolytes," *Phys. Rev. E* **100**, 042615 (2019).
- ⁶⁶L. Blum and Y. Rosenfeld, "Relation between the free energy and the direct correlation function in the mean spherical approximation," *J. Stat. Phys.* **63**, 1177–1190 (1991).
- ⁶⁷R. Roth and D. Gillespie, "Shells of charge: A density functional theory for charged hard spheres," *J. Phys.: Condens. Matter* **28**, 244006 (2016).
- ⁶⁸J. Jiang and D. Gillespie, "Revisiting the charged shell model: A density functional theory for electrolytes," *J. Chem. Theory Comput.* **17**, 2409 (2021).
- ⁶⁹R. Roth, "Fundamental measure theory for hard-sphere mixtures: A review," *J. Phys.: Condens. Matter* **22**, 063102 (2010).
- ⁷⁰A. V. Gubskaya and P. G. Kusalik, "The total molecular dipole moment for liquid water," *J. Chem. Phys.* **117**, 5290–5302 (2002).
- ⁷¹F. Booth, "The dielectric constant of water and the saturation effect," *J. Chem. Phys.* **19**, 391–394 (1951).
- ⁷²J. G. Kirkwood, "The dielectric polarization of polar liquids," *J. Chem. Phys.* **7**, 911–919 (1939).
- ⁷³E. Gongadze, U. van Rienen, V. Kralj-Iglič, and A. Iglič, "Spatial variation of permittivity of an electrolyte solution in contact with a charged metal surface: A mini review," *Comput. Methods Biomech. Biomed. Eng.* **16**, 463–480 (2013).
- ⁷⁴C. Zhang, J. Hutter, and M. Sprik, "Computing the Kirkwood g -factor by combining constant Maxwell electric field and electric displacement simulations: Application to the dielectric constant of liquid water," *J. Phys. Chem. Lett.* **7**, 2696–2701 (2016).
- ⁷⁵G. Monet, F. Bresme, A. Kornyshev, and H. Berthoumieux, "Nonlocal dielectric response of water in nanoconfinement," *Phys. Rev. Lett.* **126**, 216001 (2021).
- ⁷⁶O. V. Dolgov, D. A. Kirzhnits, and E. G. Maksimov, "On an admissible sign of the static dielectric function of matter," *Rev. Mod. Phys.* **53**, 81 (1981).
- ⁷⁷D. Andelman, "Introduction to electrostatics in soft and biological matter," in *Soft Condensed Matter Physics in Molecular and Cell Biology* (CRC Press, 2006), Vol. 6.
- ⁷⁸P. I. Ravikovitch and A. V. Neimark, "Density functional theory model of adsorption deformation," *Langmuir* **22**, 10864–10868 (2006).
- ⁷⁹P. I. Ravikovitch and A. V. Neimark, "Density functional theory model of adsorption on amorphous and microporous silica materials," *Langmuir* **22**, 11171–11179 (2006).
- ⁸⁰J. R. Henderson, "Statistical mechanics of the disjoining pressure of a planar film," *Phys. Rev. E* **72**, 051602 (2005).
- ⁸¹M. M. Hatlo, R. Van Roij, and L. Lue, "The electric double layer at high surface potentials: The influence of excess ion polarizability," *Europhys. Lett.* **97**, 28010 (2012).
- ⁸²S. Leikin, V. A. Parsegian, D. C. Rau, and R. P. Rand, "Hydration forces," *Annu. Rev. Phys. Chem.* **44**, 369–395 (1993).
- ⁸³S. Leikin and A. A. Kornyshev, "Theory of hydration forces. nonlocal electrostatic interaction of neutral surfaces," *J. Chem. Phys.* **92**, 6890–6898 (1990).
- ⁸⁴E. Gongadze, A. Velikonja, T. Slivnik, V. Kralj-Iglič, and A. Iglič, "The quadrupole moment of water molecules and the permittivity of water near a charged surface," *Electrochim. Acta* **109**, 656–662 (2013).
- ⁸⁵R. I. Slavchov and T. I. Ivanov, "Quadrupole terms in the Maxwell equations: Born energy, partial molar volume, and entropy of ions," *J. Chem. Phys.* **140**, 074503 (2014).